Dr. K. C. Tiwari

Suvan_Singh_Roy_(24_GINF_02)_INTEGRATION OF BIM MODEL WITH 3D GIS FOR CHANGE DETECTION ANALYSIS O...

PAPER

Document Details

Submission ID
trn:oid:::27535:142861073

Submission Date
Jun 13, 2026, 6:37 PM GMT+5:30

Download Date
Jun 13, 2026, 6:39 PM GMT+5:30

File Name
Suvan_Singh_Roy_(24_GINF_02)_INTEGRATION OF BIM MODEL WITH 3D GIS FOR CHANGE DETECTI....pdf

File Size
2.9 MB

57 Pages

15,178 Words

82,227 Characters

7% Overall Similarity

The combined total of all matches, including overlapping sources, for each database.

Match Groups

108 Not Cited or Quoted 7%
Matches with neither in-text citation nor quotation marks

10 Missing Quotations 1%
Matches that are still very similar to source material

0 Missing Citation 0%
Matches that have quotation marks, but no in-text citation

0 Cited and Quoted 0%
Matches with in-text citation present, but no quotation marks

Top Sources

3% Internet sources
4% Publications
5% Submitted works (Student Papers)

Match Groups

- **108** Not Cited or Quoted 7%
  Matches with neither in-text citation nor quotation marks
- **10** Missing Quotations 1%
  Matches that are still very similar to source material
- **0** Missing Citation 0%
  Matches that have quotation marks, but no in-text citation
- **0** Cited and Quoted 0%
  Matches with in-text citation present, but no quotation marks

Top Sources

3% Internet sources
4% Publications
5% Submitted works (Student Papers)

Top Sources

The sources with the highest number of matches within the submission. Overlapping sources will not be displayed.

1	Internet	researchr.org <1%
2	Student papers	University of Edinburgh on 2023-08-10 <1%
3	Student papers	AUT University on 2026-06-04 <1%
4	Student papers	University of Sydney on 2026-05-29 <1%
5	Publication	Trinh Van Hoa, Tri N.M. Nguyen, Le Van Phuc, Ngo Chau Phuong. "Integration of ... <1%
6	Student papers	Teaching and Learning with Technology on 2025-07-01 <1%
7	Student papers	AUT University on 2025-06-03 <1%
8	Internet	gs.elaba.lt <1%
9	Publication	Kharroubi, Abderrazzaq. "Semantic Segmentation For 3D Change Detection in Ur... <1%
10	Internet	www.researchgate.net <1%

11 Student papers
Consorcio CIXUG on 2023-11-13 <1%

12 Internet
www.peeref.com <1%

13 Publication
Halil İbrahim Şenol, Türkay Gökgöz. "Integration of Building Information modelin... <1%

14 Student papers
Queen's University of Belfast on 2024-09-06 <1%

15 Publication
James H. Churnside, Richard D. Marchbanks, Svein Vagle, Shaun W. Bell, Phyllis J. ... <1%

16 Publication
Rita Machete, Ana Paula Falcão, M. Glória Gomes, A. Moret Rodrigues. "The use of... <1%

17 Student papers
University of Glasgow on 2025-05-28 <1%

18 Internet
doaj.org <1%

19 Internet
www.mdpi.com <1%

20 Student papers
Politecnico di Milano on 2020-06-13 <1%

21 Student papers
University of Worcester on 2014-10-28 <1%

22 Student papers
Brunel University on 2023-09-01 <1%

23 Internet
ir.vnulib.edu.vn <1%

24 Publication
Francisco López-Herrera, Jaime González Maiz Jiménez, Adán Reyes Santiago. "Dir... <1%

25 Student papers

Louisiana State University on 2026-04-15 <1%

26 Publication

Rajit Gupta, Laxmi Kant Sharma. "Mapping Canopy Height from ICESat-2 and Lan... <1%

27 Student papers

INholland on 2025-09-17 <1%

28 Publication

Rachna Gangwar, Anurima Mukherjee Basu. "Emerging Agenda in Sustainable Inf... <1%

29 Student papers

Sunway College on 2006-04-26 <1%

30 Student papers

University of Newcastle upon Tyne on 2024-10-14 <1%

31 Student papers

Vrije Universiteit Amsterdam on 2025-07-25 <1%

32 Internet

arxiv.org <1%

33 Internet

isprs-archives.copernicus.org <1%

34 Student papers

Indian Institute of Technology, Bombay on 2018-09-06 <1%

35 Publication

Luqi Zhang, Zhihua Zhang, Jiuyan Zhang, Xin Qiao, Zhenchao Zhang, Bisheng Yan... <1%

36 Student papers

University of College Cork on 2015-09-07 <1%

37 Student papers

University of Melbourne on 2025-04-11 <1%

38 Internet

books.fupress.com <1%

39 Internet

eprints.kfupm.edu.sa <1%

40 Publication

Uwe Stilla, Yusheng Xu. "Change detection of urban objects using 3D point clouds... <1%

41 Publication

Bao Rong Chang, Hsiu Fen Tsai. "Applying Visual Image and Satellite Positioning f... <1%

42 Student papers

Macquarie University on 2016-06-03 <1%

43 Student papers

Universidad de La Laguna on 2019-09-17 <1%

44 Internet

open.library.ubc.ca <1%

45 Internet

transfer.hft-stuttgart.de <1%

46 Student papers

University of Newcastle upon Tyne on 2015-04-17 <1%

47 Internet

itcon.org <1%

48 Internet

link.springer.com <1%

49 Internet

publicationslist.org <1%

50 Student papers

Florida State University on 2026-04-22 <1%

51 Student papers

Massey University on 2025-05-09 <1%

52 Student papers

Universiti Teknologi Malaysia on 2024-03-13 <1%

53 Student papers
University of Nottingham on 2016-05-06 <1%

54 Internet
clickdown.org <1%

55 Internet
openaccess.hacettepe.edu.tr:8080 <1%

56 Publication
"Disaster Prevention and Mitigation of Infrastructure", Springer Science and Busi... <1%

57 Publication
Carneiro, Joel Márcio Torres. "Virtual/Augmented Reality for Infrastructure Mana... <1%

58 Publication
Michael H. Wimmer, Gottfried Mandlburger, Camillo Ressl, Norbert Pfeifer. "Strip ... <1%

59 Publication
Mustafa Zeybek. "Integrating advanced remote sensing technologies and machin... <1%

60 Publication
Sensor Review, Volume 20, Issue 3 (2006-09-19) <1%

61 Student papers
Universiti Teknologi Brunei on 2026-04-02 <1%

62 Student papers
University of Central Lancashire on 2022-04-07 <1%

63 Student papers
University of Portsmouth on 2025-08-28 <1%

64 Internet
eprints.gla.ac.uk <1%

65 Internet
isprs-annals.copernicus.org <1%

66 Internet
jmr.cmsjournal.net <1%

67 Internet

zero.sci-hub.se <1%

68 Student papers

Oxford Brookes University on 2025-05-10 <1%

69 Student papers

University of Auckland on 2023-10-11 <1%

70 Student papers

University of Durham on 2024-04-19 <1%

71 Publication

Albouraee, Walaa Taha Ahmed. "A Digital Record System For Heritage Buildings i... <1%

72 Publication

G. Vacca, E. Quaquero, D. Pili, M. Brandolini. "INTEGRATING BIM AND GIS DATA T... <1%

73 Student papers

Manipal Academy of Higher Education (MAHE) on 2026-03-15 <1%

74 Student papers

The Hong Kong Polytechnic University on 2019-11-27 <1%

75 Student papers

Universiteit Utrecht on 2025-11-26 <1%

76 Student papers

University of Northumbria at Newcastle on 2016-05-03 <1%

77 Publication

Wen Xiao, Hui Cao, Miao Tang, Zhenchao Zhang, Nengcheng Chen. "3D urban obj... <1%

CHAPTER 1

INTRODUCTION

At its core, construction is about turning intent into physical reality. A building begins as a sequence of drawings, models and specifications, a precise articulation of what should be, and over months or years of work on site that intent is slowly given form in concrete, steel and glass. “There has always been concern in the industry about the gap between what was intended and what was actually built. It is rarely zero. Materials don’t always behave the way you think they will, site conditions place limitations you didn’t quite anticipate, and the sum of the small choices made by workers and supervisors in the field can result in a building that is different, sometimes in subtle ways, sometimes in major ways, than what the designer intended. A constant challenge for construction management is to identify these deviations early, accurately and without excessive manual effort.

For most of the history of the built environment industry this was checked by the naked eye, with measuring tapes, total stations and the odd site visit by an engineer or inspector. These methods are not without value an experienced engineer can spot a poorly cast column or a misaligned beam relatively quickly but they are slow, spatially incomplete, and highly dependent on the individual conducting the inspection. A site visit captures a snapshot of a small portion of the structure at a single point in time. What it cannot do, practically speaking, is produce a comprehensive, spatially continuous record of how the entire built structure compares with the original design. For large and complex infrastructure projects airports, rail terminals, stadiums, multi-storey commercial buildings that limitation becomes increasingly costly.

1.1 The Emergence of Digital Twins and 3d Data

The past two decades have seen a fundamental shift in how buildings and infrastructures are designed, documented & managed. Building Information Modeling BIM emerged as a response to the fragmentation and information loss that had long plagued the construction industry. Rather than working from a collection of two-dimensional drawings that needed to be mentally assembled into a three-dimensional picture, BIM introduced the idea of a single, intelligent, parametric model that contains not just geometry but also embedded information about materials, structure, systems, and schedules. This model is the single source of the true design intent through the entire life cycle of the project.

BIM is often described in terms of dimensions, where each dimension represents a level of information on top of basic three-dimensional geometry. The three main spatial dimensions X,Y & Z defining shape of model in physical space. Time is introduced as a fourth dimension to link elements of the model to construction schedules and to allow the simulation of the construction sequence. The fifth dimension adds cost and enables quantities to be extracted and budgets to be tracked against the changing model. Besides

these, a sixth dimension concerns facility management and lifecycle performance and a seventh dimension concerns sustainability and environmental impact data. In practice, most construction projects are working mainly in the 3D to 5D spaces but the conceptual framework shows how BIM has evolved from a visualization tool to a full project intelligence platform (Ma & Ren, 2017).

63

Hence, Geographic Information Systems GIS became a platform for capturing, managing and analysing of spatially referenced information about the real world. BIM is primarily concerned with the scale of a single building or structure whereas GIS operates at urban, regional and global scales and combines data about terrain, infrastructure networks, land use and built assets within a single georeferenced coordinate framework. The distinction between the two has historically been stark: BIM models are accurate and information-rich, but lack real-world positioning, whereas GIS datasets are geospatially accurate but often lack the level of geometric and semantic detail found in BIM. There is research and industry practice in the convergence of these two paradigms, BIM and GIS, as it is realized that the strengths of each can compensate for the weaknesses of the other (Biljecki et al., 2017 and Ma & Ren, 2017).

Three-dimensional GIS, in particular, has gained significant traction as a medium for representing the as-built state of structures. Advances in drone-based photogrammetry and terrestrial or aerial LiDAR scanning have made it possible to capture dense, geometrically accurate three-dimensional point clouds of physical structures at a fraction of the cost and time that traditional survey methods would require. A modern drone survey of a mid-sized building can be completed in a matter of hours and produce tens of millions of georeferenced points, each representing a measured location on the surface of the structure. This as-built data, when processed and integrated into a GIS environment, creates a spatially accurate representation of the structure as it exists not as it was designed to exist (Chiabrando et al., 2020; Shakeri et al., 2024).

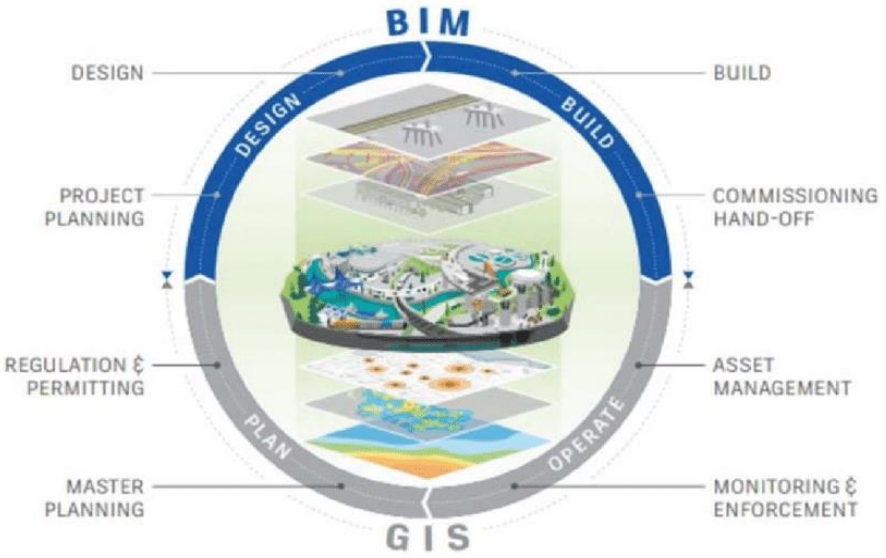


Figure 1.1: Conceptual GIS and BIM integration cycle.

27 https://www.researchgate.net/figure/GIS-and-BIM-integration-cycle-https-blogsautodeskcom_fig2_350359362

1.2 The Problem of Change Detection

When both a BIM model and a 3D GIS representation of the same structure exist, the natural and valuable question is: where do they differ, and by how much? This question sits at the heart of what is broadly called change detection the identification of geometric, spatial, or semantic differences between two representations of the same object, captured at different times or derived from various sources.

The first is deviation from the as-designed that is whether the physical structure captured by scanning matches the geometry of the BIM model within acceptable tolerances. A wall moved a few millimeters is usually not a problem, one moved several centimeters in a structurally critical location may be. The second concern is the monitoring of construction progress using the BIM model in comparison with the as-built scan to identify which portion of the designed structure has been built. This is especially true in large projects where visual assessment of overall progress is difficult and where reporting impacts on payments, scheduling and resource allocation progress. A third concern is plan change identification / identifying instances where the built structure is different from the design not because of construction error, but because of intentional changes made on site that was not captured in a formal design revision (Xiao et al., 2023). Such undocumented or unauthorized changes, sometimes referred to as as-built 13 divergences, pose a serious risk in later phase of a project's life cycle, such as during renovation, structural assessment or facility management.

Each of these concerns has practical consequences. Deviations that go undetected during construction become harder and more expensive to rectify as the project progresses. Progress that is inaccurately reported can distort financial planning and delay downstream activities. Undocumented plan changes, if not caught early, can compromise structural safety, violate regulatory requirements, or lead to costly conflicts during the operational stage of a building's life. Having a reliable, automated method for detecting and quantifying these differences is therefore not merely an academic exercise it has direct implications for project outcomes, safety, and cost.

Table 1.1: BIM vs. 3D GIS.

ASPECT	**BIM**	**3D GIS**
Represents	Design intent : as planned	Physical reality : as built
Data source	Design software (e.g. Revit)	Drone / LiDAR scanning
Working scale	Building / component level	Site / geographic level
Coordinates	Local model space	Georeferenced (GPS / UTM)
Element information	Rich : walls, columns, slabs, roof, etc. labelled	None : geometry only, no semantic labels
Accuracy	Sub-millimetre (designed)	Centimetre-level (measured)
Key limitation	Does not reflect what was actually built	Does not know what each surface should be
Role in this study	*Reference surface for comparison*	*As-built surface for comparison*

1.3 Scope and Motivation of the Study

This thesis develops and applies a framework for the BIM–GIS integration specifically designed for change detection in building construction. The main case study is the Bhogumpura Airport terminal building, which is large and complex enough to test the methodology in real world conditions. However, the framework is intentionally general rather than site-specific. The BIM model is the design reference that is exported as a geometric mesh from the design authoring software. A 3D GIS model of the structure based on photogrammetric or LiDAR data acquisition serves as an as-built reference. Both are processed, aligned and compared via a single computational pipeline. What differentiates this work from simpler point cloud comparison approaches is the attention paid to the semantic content of the BIM model. Instead of considering the BIM geometry as a homogeneous surface, the framework classifies each region of the BIM geometry according to architectural element type walls, columns, slabs, roof surfaces, ceiling elements, openings, and beams based on material group data embedded in the exported model file. Therefore, statistics on deviations can be reported not only globally for the whole structure but also separately for each class of elements. For example, a project team can then see that the roof surface is largely conforming while the column positions show moderate deviations a distinction that has direct implications for what corrective action, if any, is needed.

The framework also yields an estimate of construction progress through quantifying the coverage of the BIM surface with the as-built scan data . The deviations are statistically classified with a sigma-based scheme that gives a more nuanced picture than a simple pass/fail threshold. The outputs are communicated through colour-coded visualizations, spatial hotspot maps, per-element deviation charts and structured report formats that are intended to be useful to not only researchers but also practicing engineers and project managers who need to act on the information.

The larger implications of this kind of work are much larger than any single project. As the construction industry is moving towards higher levels of digitization with BIM adoption becoming a regulatory requirement in a number of countries and drone surveying becoming routine on major sites, the tools for making sense of the data that these technologies produce are becoming more and more important (Cepa et al., 2024 and Ma & Ren, 2017). A methodology that can systematically compare design intent to physical reality, flag deviations by severity and element type, estimate construction progress, and detect undocumented plan changes, all from existing digital outputs, has the potential to materially improve the way that construction projects are monitored and managed.

1.4 Review of Literature

1. Integration of BIM and GIS for managing infrastructure project: A Case Study of the 3/2 street in Kien Giang, Vietnam

Trinh Van Hoa, Tri N. M. Nguyen, Le Van Phuc, Ngo Chau Phuong (2025);

The integration of Building Information Modeling (BIM) and Geographic Information Systems (GIS) for better management of transportation infrastructure projects is studied in this paper.

The case study of 3/2 road project in Kien Giang, Vietnam was used as an example to demonstrate the integration process by using the tools of Revit, Civil3D and ArcGIS Pro. The method involves converting the BIM models (IFC) into GIS compatible formats and merging them into the WebGIS platform, to combine spatial and design data.

The results show that BIM–GIS integration enhances project planning, design coordination, asset management and decision-making throughout the infrastructure lifecycle. The study also highlights the challenges of data standardization, coordinate system compatibility and high upfront implementation costs.

Limitation:

The research is primarily focused on integration and visualization for infrastructure management, but does not address automated 3D change detection, or comparison of as-built vs. as-designed models.

8

2. Integration of Building Information Modeling (BIM) and Geographic Information System (GIS): A New Approach for IFC to CityJSON Conversion

Halil İbrahim Şenol and Türkay Gökgöz (2024);

53

The study proposes a new approach for the integration of BIM and GIS by converting IFC data to CityJSON format, to improve interoperability between building models and geospatial systems.

The research tackles an important challenge of BIM–GIS integration: information loss in terms of semantics and geometry during data transformation between the two platforms of BIM and GIS. The authors developed an algorithm based on programming language Python using semantic linked data and JSON-LD technologies to preserve the attribute of building components in the conversion process.

13

The proposed method achieved almost 95% accuracy in retaining semantic information in the conversion of IFC to CityJSON.The approach improves data interoperability for smart city applications, urban planning and 3D city model development.

Limitation:

This study mainly addresses on data conversion and semantic interoperability but does not consider the 3D change detection between as-built and as-designed models nor construction monitoring with UAV/LiDAR data.

68

3. Integration of BIM and GIS for Construction Progress Monitoring Using UAV Photogrammetry

Francesco Chiabrando, Filippo Maria Prandi, and Francesco Spanò (2020);

62

The study explores the integration of BIM and GIS with UAV photogrammetry to support construction progress monitoring and site management.

3
3

Photogrammetric processing was used in generating point clouds and 3D mesh of the construction site from the UAV imagery. Thus, the generated models were integrated with BIM data and GIS platform to allow for spatial analysis and visualization of construction progress.

The results show that integrating UAV-derived 3D models with BIM and GIS enhances progress monitoring, documentation, and decision-making in construction projects. The integrated approach enables the stakeholders to visualize the construction status and compare the planned vs actual site conditions.

Limitation:

Although the main emphasis on this study is on visualizing of construction progress, automated geometric deviation analysis or quality assessment based on LiDAR-derived 3D GIS models has not been implemented.

28 73

4. Integration of 3D GIS and BIM for Visual Detection of Concealed Facilities

Wang et al. (2018);

10

This study shows a method for the integration of Building Information Modeling (BIM) and 3D GIS for better visualizing and managing of underground and hidden infrastructure facilities.

BIM helps providing detailed building component information and 3D GIS provide spatial context and georeferencing capability for large scale urban environments.

The study presents a data integration framework for the seamless transfer of information between BIM models and GIS platforms. The integrated system helps in conflict detection and identification of hidden facilities like pipelines and utilities in complex infrastructure environments.

Limitation:

The study is mostly focused on visual detection and infrastructure management. It does not perform automated 3D change detection or deviation analysis between planned BIM models and real world captured data.

18

5. Integration of 3DGIS and BIM and Its Application in Visual Detection of Concealed Facilities

Xiaoyu Wang and Mingxia Xie (2024);

45

This research proposes an integration framework between Building Information Modeling (BIM) and 3D Geographic Information Systems (3DGIS) for visualization and management of concealed building facilities.

The methodology uses the data standards of IFC and CityGML for interoperability between BIM models and GIS platforms. Techniques such as semantic mapping, coordinate transformation and geometric simplification were used to convert BIM data into formats compatible with GIS.The integrated 3D environment enables accurate spatial visualization and detection of hidden building infrastructure, such as pipelines and utilities.

The results indicate that BIM–GIS integration can enhance facility management, spatial analysis, and decision making in the operation and maintenance of buildings.

57

Limitation:

The study focuses mainly on visual detection and facility management, but it does not implement automated change detection between BIM design models and real-world 3D GIS models from UAV/LiDAR data.

6. BIM–GIS Integration for Supporting Geospatial Applications

Mohammad Biljecki, Hugo Ledoux, and Jantien Stoter (2017);

In this paper we study the integration of Building Information Modelling (BIM) and Geographic Information Systems (GIS) for geospatial analysis and urban applications.

The research underlines the inconsistencies between BIM data models (IFC) and GIS standards such as CityGML that lead to interoperability problems. The proposed framework aims to make BIM data compatible with GIS, allowing to use building models in geospatial environments. The integrated approach allows to perform 3D city modelling, spatial analysis and to improve the management of urban infrastructure.

The paper stresses the importance of semantic mapping and geometric transformation in linking BIM objects to GIS features.

Limitations:

The study mainly addresses the issues of conceptual BIM–GIS integration and interoperability. It doesn't carry out the real-world change detection and comparison between the BIM design models and the 3D GIS models generated from UAV or LiDAR data.

7. Automated Construction Progress Monitoring Using UAV and BIM Integration

Ali Shakeri, Mahdi Golparvar-Fard, and Burcin Becerik-Gerber (2024);

The study examined the use of UAV based reality capture combined with Building Information Modelling (BIM) for automated construction progress monitoring.

The UAV imagery is processed through photogrammetry techniques to create dense point clouds and 3D models that represent real conditions on the construction site.These generated 3D models are compared with BIM design models to identify the differences between the planned and as-built structures.The integration enables tracking of construction progress, identification of deviations and project management improvement.

The research shows that the combination of UAV and BIM enhances the efficiency of construction monitoring and offers accurate visual records of project progress.

Limitations:

The study mainly relies on the progress monitoring by UAV photogrammetry, but does not involve the integration of 3D GIS environment or LiDAR based models for more accurate change detection and spatial analysis that can further improve the construction monitoring and quality assessment.

8. BIM–GIS Integration for Infrastructure Digitalization and Facility Management

Juan José Cepa, María G. Alberti, Rafael M. Pavón and Juan A. Caballero (2024);

The paper explores the integration of Building Information Modelling (BIM) and Geographic Information Systems (GIS) to support digital transformation in the Architecture, Engineering, Construction and Operation (AECO) sector.

BIM provides detailed information about infrastructure and GIS provides large scale spatial context, so they are complementary technologies for infrastructure management. The research is a case study of the Madrid Calle-30 ring road, where BIM models were incorporated into a GIS environment using the IFC and SLPK formats. The integrated system stores the information in an external database, which allows updates and management of infrastructure data without directly modifying the 3D model.

The approach helps in facility management, infrastructure monitoring and better decision making over the lifecycle of infrastructure assets.

Limitation:

The study focuses mainly on BIM–GIS interoperability and infrastructure management, but it does not implement automated 3D change detection between BIM design models and UAV/LiDAR-derived real-world 3D GIS models, which is the focus of the proposed research.

9. 3D Urban Object Change Detection from Aerial and Terrestrial Point Clouds: A Review

Wen Xiao, Hui Cao, Miao Tang, Zhenchao Zhang, and Nengcheng Chen (2023);

The study reviews 3D change detection methods for urban environments using point clouds from aerial and terrestrial sensors.

It focuses on detecting changes in buildings, street scenes, urban trees, and construction sites for urban monitoring and planning. The paper discusses data sources such as LiDAR and Structure-from-Motion (SfM) used to generate multi-temporal 3D point clouds. Change detection approaches are categorized into point-level, voxel-level, segment-level, and object-level methods.

The study also highlights machine learning and deep learning techniques for improving automated change detection accuracy.

Limitation:

The study mainly reviews general 3D point cloud change detection techniques and does not focus on direct comparison between BIM design models and 3D GIS/UAV-derived models for construction monitoring.

10. Automatic 3D Change Detection for Urban Environments Using Multi-Temporal Point Clouds

R. Qin, X. Tian, and D. Gruen (2020);

The study presents an automatic method for detecting 3D changes in urban environments using multi-temporal point cloud data.

The method is based on the detection of the changes of buildings and other urban objects in time using LiDAR and photogrammetric point clouds. The method is based on a point cloud comparison and spatial analysis for the detection of additions, removals and structural changes.The research findings show that change detection using 3D point clouds can be useful for urban monitoring, infrastructure management and city planning.

Experimental results demonstrate the effectiveness of the method in detecting urban changes with better accuracy than traditional 2D approaches.

Limitation:

The study focuses mainly on point cloud-based urban change detection and does not involve BIM models with 3D GIS data for comparing design with reality or for monitoring construction progress.

11. Integrated Application of BIM and GIS: An Overview

Zhiliang Ma and Yuan Ren (2017);

This paper provides an overview of the current research on the integration of Building Information Modelling (BIM) and Geographic Information Systems (GIS) for smart city and infrastructure applications.

The paper analyses previous studies according to the application object, lifecycle phase, integration pattern and software platforms used for BIM–GIS integration.

Results show that most BIM–GIS applications focus on buildings, while fewer studies address infrastructure and urban district applications. The research highlights that integration is commonly achieved by transferring BIM data into GIS platforms such as ArcGIS or other visualization systems. The study emphasizes that BIM–GIS integration

can support urban planning, facility management, hazard analysis, and smart city development.

Limitation:

The paper mainly provides a review of BIM–GIS integration concepts and applications, but it does not address 3D change detection or comparison between BIM design models and UAV/LiDAR-derived GIS models for monitoring construction changes.

12. Object-Based 3D Building Change Detection Using Point-Level Change Indicators

Luqi Zhang, Zhihua Zhang, Jiuyan Zhang, Xin Qiao, Zhenchao Zhang, Bisheng Yang, and Zhen Dong (2023);

The study proposes an object-based 3D building change detection method using multi-temporal airborne laser scanning (ALS) point clouds.

Point-level change indicators are calculated from geometric differences between point clouds from two time periods to detect structural changes. A region-growing and graph-cut segmentation approach is used to extract building objects from the point cloud data. The detected building objects are analyzed using object-level features and classified with a Random Forest model to determine change types.

Experimental results show high performance with precision of 91.1% and recall of 85.3% on real ALS datasets for detecting building changes.

Limitation:

The method focuses on point cloud–based building change detection, but it does not integrate BIM design models with GIS or UAV-derived 3D models for comparing planned and actual construction structures.

13. Deep Learning Framework for Hyperspectral Image Change Detection Using Spatial–Temporal Modeling

Luqi Zhang, Zhihua Zhang, Jiuyan Zhang, Xin Qiao, Zhenchao Zhang, Bisheng Yang, and Zhen Dong (2025);

The study proposes a deep learning framework for hyperspectral image change detection using multi-temporal hyperspectral datasets.

A spatial–temporal modeling approach is used to capture both spectral and spatial information from hyperspectral images acquired at different time periods.Deep convolutional neural networks are employed to extract discriminative spectral-spatial features and learn complex patterns of change between the two images. The model

utilises temporal differences in hyperspectral signatures to better detect subtle changes in land cover and surface.The framework improves detection accuracy by reducing noise and enhancing meaningful change features in hyperspectral scenes.

Limitation:

The method focuses mainly on hyperspectral image–based change detection and does not integrate other geospatial data sources such as LiDAR point clouds, UAV imagery, or BIM models for more comprehensive structural change analysis.

Table 1.2: Review of related literature.

	Authors and year	**Focus area**	**Key contribution**	**Limitation / Gap**
1	Trinh Van Hoa et al. (2025)	BIM–GIS integration	Revit + ArcGIS Pro for road project management; WebGIS for spatial and design data	No automated 3D change detection or as-built vs as-designed comparison
2	Şenol and Gökgöz (2024)	BIM–GIS integration	IFC to CityJSON conversion with 95% semantic accuracy using Python + JSON-LD	No 3D change detection or construction monitoring using UAV/LiDAR
3	Chiabrando et al. (2020)	Progress monitoring	UAV photogrammetry + BIM + GIS for construction site progress monitoring and visualisation	No automated geometric deviation analysis or LiDAR-based quality assessment
4	Wang et al. (2018)	BIM–GIS integration	BIM + 3D GIS framework for visualisation and detection of concealed underground facilities	No automated deviation analysis between BIM and real-world captured data
5	Wang and Xie (2024)	BIM–GIS integration	IFC + CityGML semantic mapping and coordinate transformation for concealed facility	No change detection between BIM design models and UAV/LiDAR

			management	as-built data
6	Biljecki et al. (2017)	BIM–GIS integration	IFC to CityGML framework for 3D city modelling, spatial analysis, and urban management	Conceptual only; no real-world change detection or as-built comparison implemented
7	Shakeri et al. (2024)	Progress monitoring	UAV photogrammetry + BIM for automated construction progress tracking and deviation identification	No 3D GIS environment or LiDAR integration for enhanced spatial change detection
8	Cepa et al. (2024)	BIM–GIS integration	IFC + SLPK for infrastructure digitalization and lifecycle facility management (Madrid ring road)	No automated 3D change detection using UAV or LiDAR-derived GIS models
9	Xiao et al. (2023)	3D change detection	Review of LiDAR + SfM point cloud change detection methods for urban environments	Review only; no BIM-to-GIS comparison or construction monitoring framework
10	Qin et al. (2020)	3D change detection	Automatic 3D urban change detection using multi-temporal LiDAR and photogrammetric point clouds	No BIM model integration or design-to-reality comparison for construction monitoring
11	Ma and Ren (2017)	BIM–GIS integration	Overview of BIM–GIS applications across smart city, urban planning, and facility management	Conceptual review only; no 3D change detection or UAV/LiDAR -based

			domains	monitoring
12	Zhang et al. (2023)	3D change detection	Object-based 3D building change detection from ALS point clouds 91.1% precision, 85.3% recall	No BIM model integration for design-to-reality comparison or construction monitoring
13	Zhang et al. (2025)	3D change detection	Deep learning + spatial–temporal modelling for hyperspectral image change detection	Hyperspectral only, no LiDAR, UAV, or BIM integration for structural change analysis

1.5 Need of Research

Large infrastructure projects require accurate monitoring of construction progress and structural deviations, which cannot always be achieved through traditional inspection methods.

BIM models represent the planned design, but project managers often lack tools to automatically compare the design with the actual structure built on site.

UAV photogrammetry and LiDAR enable rapid generation of 3D GIS models of construction sites, creating an opportunity for design-to-reality verification.

By integrating BIM models with 3D GIS data captured by UAVs allows the identification of construction deviations, missing elements or dimensional errors.

A workflow including point cloud sampling, ICP registration and distance based change detection allows quantitative deviation analysis.

This kind of system can be used for construction progress monitoring, quality assessment and decision making in large infrastructure projects undertaken by companies like Larsen & Toubro.

1.6 Research Gap

Although many studies are devoted to BIM–GIS integration for visualisation and data management, very few efforts are devoted to the automated geometric comparison of BIM design models and real-world 3D GIS models.

However, current 3D change detection techniques are mostly applied to multi-temporal point clouds comparison rather than planned BIM models and as-built 3D models.

Most of the construction monitoring techniques are based on a manual site inspection which is time consuming and may not be able to detect small structural deviations.

UAV-based photogrammetry and LiDAR can generate accurate 3D site models, but these datasets are rarely integrated with BIM to perform design-to-reality deviation analysis.

Limited research exists on point cloud alignment and deviation analysis workflows (ICP-based registration and distance computation) specifically for construction quality assessment.

There is a lack of automated frameworks that can generate deviation maps and change detection results directly from BIM and UAV-derived models.

1.7 Research Objectives

- To generate or procure 3D GIS model and BIM model of a building.
- To convert BIM and 3D GIS mesh models into comparable point cloud datasets through uniform mesh sampling and preprocessing like Gaussian Filter.
- To perform accurate spatial alignment between BIM and GIS point clouds using a multi-stage Iterative Closest Point (ICP) registration method with region-based cropping.
- To compute geometric deviations between the planned BIM model and the as-built GIS model using point-to-point distance analysis.
- To detect and classify structural changes using Z score-based deviation analysis and generate 3D deviation map for construction progress monitoring and quality assessment.

CHAPTER 2
STUDY AREA

2.1 Location and Regional Setting

The area of focus of this study is Alluri Sitarama Raju International Airport, commonly referred to as Bhogapuram Airport. The project is located in Bhogapuram mandal, Vizianagaram district, in the state of Andhra Pradesh, India. Geographically, the site lies at approximately 18.0°N latitude and 83.5°E longitude, along the National Highway 16 corridor, roughly 45 kilometers north of Visakhapatnam city. Figure 2.1 shows the location of the study area in the regional context.

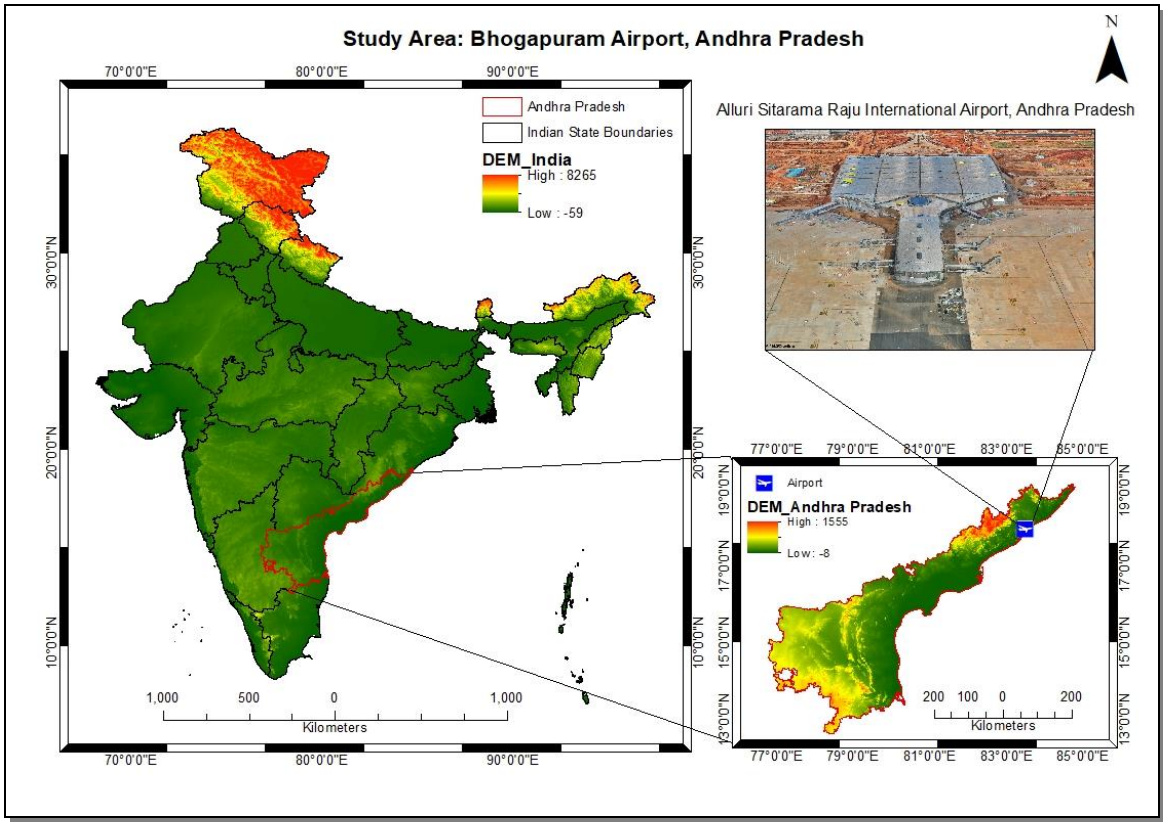


Figure 2.1: Study Area: Bhogapuram Airport, Andhra Pradesh.

The broader region in which the airport is situated the North Andhra coastal belt encompasses the districts of Vizianagaram and Srikakulam, and extends towards the southern boundary of Odisha. Historically, this region has depended entirely on Visakhapatnam Airport for air connectivity, which has placed increasing strain on that facility as regional travel demand has grown. Some of this imbalance was to be resolved by the Bhogapuram Airport project, which was conceived to provide dedicated air infrastructure closer to a long-underserved population and economic base.

2.2 Project Background and Significance

28

Bhogapuram Airport is a green field project, meaning it is being developed from the ground up on a site that previously did not have any aviation infrastructure. The project is being developed as a public-private partnership and is expected to operate as an international airport upon completion, with a terminal building capable of handling several million passengers a year. The scale of the project, hundreds of acres of mostly agricultural and open land, puts it squarely in the category of major infrastructure projects, where complexity of construction and risk of design-to-build discrepancies are both high.

The terminal building, the subject of this study, is a structurally complex facility incorporating load bearing walls, roof structures of varying geometry, structural columns, floor and ceiling systems and extensive glazed facades. This kind of architecture is important from a research point of view as it guarantees the change detection analysis to be performed on a really diverse set of structural element types, rather than a repetitive or geometrically simple form, which would limit the scope and the credibility of the results.

2.3 Physical Characteristics of the Site

Bhogapuram is situated on flat terrain typical of the low-lying coastal alluvial plain that dominates much of this stretch of India's eastern seaboard. The elevations across the site vary only slightly and there is no significant topographical relief. At the time of study, the surrounding landscape included active construction zones, cleared land, developing access roads, and patches of residual natural cover at the periphery of the site. The absence of steep gradients or complex natural terrain features simplifies some aspects of spatial analysis while the construction activity itself with equipment, temporary structures, and partially completed building elements introduces its own complexity into any three-dimensional survey of the site.

The site enjoys good climatic conditions for aerial survey operations, typical of the coastal tropical climate of the region warm temperatures, moderate humidity, and relatively predictable seasonal patterns outside of the monsoon months. Survey campaigns conducted outside the June to September period generally benefit from stable atmospheric conditions and good visibility, both of which are relevant to the quality of photogrammetric data capture.

2.4 Suitability for this Research

Several characteristics of Bhogapuram Airport make it a well-suited case for the objectives of this study. Its greenfield nature means there is a clean, unambiguous design baseline the BIM model represents exactly what should be built, with no pre-existing conditions to account for. The ongoing construction status at the time of data acquisition means the site presents a live scenario where deviations, partial completions, and

undocumented changes may all coexist precisely the conditions under which a change detection framework needs to prove its usefulness.

Also, the project's scale and strategic significance make it relevant in practical terms. At a facility of this kind, a construction alignment error or a significant structural deviation has real consequences for safety, for compliance with regulatory requirements, and for the long-term operational performance of the airport. The ability to detect such issues early, systematically and over the full extent of the structure is not an academic abstraction at a site like this, it is a real operational need.

While the specific subject of analysis in this dissertation is the Bhogapuram terminal building, the research is conceived with broader applicability. Airport terminals, railway stations, hospitals, stadiums and large institutional buildings share many of the same qualities structural complexity, large footprints, multiple element types, prolonged construction timelines that make systematic monitoring both challenging and important. The site is representative and credible of that wider class of infrastructure and findings from this study are expected to be transferable beyond this particular project.

CHAPTER 3
DATA AND METHODS

This Chapter will contains the detailed knowledge about the data used for preparation of this report and the methods used for doing the Assessments.

3.1 Data Used

The study mainly relies on two datasets; BIM model of the Bhogapuram Airport terminal building and 3D GIS model of the same building created from a drone-based aerial survey. Each dataset represents the building from a fundamentally different perspective: the BIM model represents what the structure was intended to be, while the GIS model represents what it actually looks like on site at the time of survey. The characteristics of both datasets are summarized in **Table 3.1**.

Table 3.1: Data Used, GSD = Ground Sampling Distance, AGL = Above Ground Level, GCP = Ground Control Point, MTL = Material Library file associated with OBJ format.

Parameter	BIM Data	3D GIS Data (Drone Survey)
Data source	Autodesk Revit: design model by project consultant	RFly drone: aerial photogrammetric survey
Sensor / payload	—	RGB Camera and LiDAR: 0.05 m GSD resolution
Flight altitude	—	50 m AGL (above ground level)
Survey area	Terminal building: 62,500 m² gross floor area	Terminal building footprint and immediate surroundings
Ground control points	—	5 GCPs: used for georeferencing and accuracy control
Processing software	Autodesk Revit	Agisoft Metashape: photogrammetric reconstruction
Output format	OBJ mesh with MTL material groups (element classes embedded)	OBJ mesh: 3D building model only
Coordinate system	Local model space	WGS84: Geographic (EPSG:4326)

3.1.1 BIM Model

The BIM model was created in Autodesk Revit by the project design consultant as part of the design documentation for the terminal building. It was exported in OBJ format a widely supported mesh exchange format with an accompanying MTL (material library file) in which Revit assigns named material groups corresponding to architectural element categories. These material group names referencing walls, columns, roof surfaces, floor slabs, ceiling elements, beams, windows, doors, and miscellaneous components are retained in the exported file and form the basis for element-level classification in the change detection analysis. The BIM model exists in a local model coordinate space with no inherent georeferencing, which means it must be spatially registered to the GIS dataset before any geometric comparison is possible.

3.1.2 3D GIS Model

The as-built 3D model of the terminal building was obtained through an aerial survey conducted using an RFly drone equipped with two sensors an RGB camera and a LiDAR sensor. The RGB camera took high resolution images of the terminal building surface with a ground sampling distance of 0.05 metres. The LiDAR sensor enabled direct geometric measurements of the structure simultaneously, thus yielding dense point cloud data that are independent of image texture and lighting. The survey was carried out at an altitude of 50 m above ground level, and five ground control points were set up over the terminal building area before the flight, to facilitate georeferencing of the reconstructed model.

The captured data was processed in Agisoft Metashape, which performed image alignment, dense point cloud generation and mesh reconstruction from the combined RGB and LiDAR input. The output of this process is a 3D OBJ mesh of the terminal building georeferenced in the WGS84 geographic coordinate system (EPSG: 4326). Unlike the BIM model, the GIS mesh does not contain semantic information on the types of elements it represents, and is just a representation of surface geometry without any inherent knowledge of which surfaces represent walls, columns or roof elements.

It is worth noting that both datasets, despite representing the same physical structure, arrive in different coordinate systems and at different levels of geometric detail. Bridging these differences through reprojection, scaling, noise filtering, and spatial registration is the first major task of the processing pipeline described in the sections that follow.

3.2 Methodology

The methodology section is divided into three parts based on the components of this project, i.e. building of the BIM model from Autodesk Revit, generation of 3D GIS model in Agisoft Metashape and lastly Change Detection using Python;

3.2.1 Building of BIM Model

The BIM model used in this study was created using Autodesk Revit, a parametric building information modeling platform widely adopted in the architecture, engineering, and construction industry (Cepa et al., 2024 and Trinh Van Hoa et al., 2025). The model represents the terminal building of Bhogapuram Airport as designed, and serves as the geometric reference against which the as-built GIS data is compared. The creation process followed a structured sequence of steps, as shown & described in Figure 3.1 below;

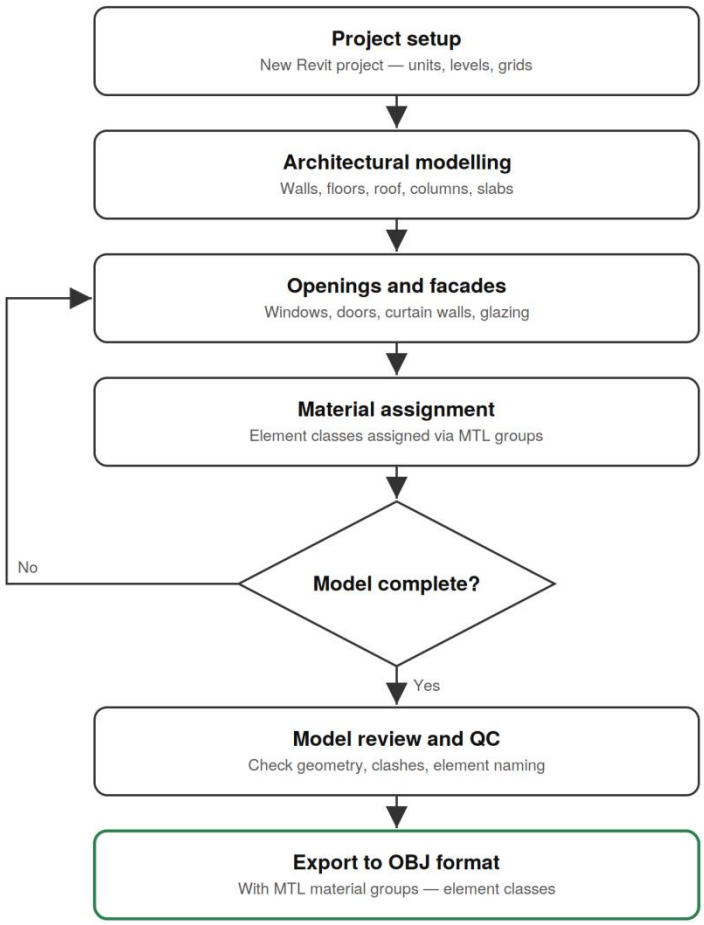


Figure 3.1: BIM model creation workflow in Autodesk Revit.

The process starts with project setup, which includes establishing a new Revit project file with the correct units, floor levels, and structural grids that match the actual building layout. This defines the spatial setting for all subsequent modelling. At this stage a correct set-up is essential, because any errors in the definition of levels or in the grid alignment propagate through the whole model and are difficult to correct at a later stage.

The main architectural elements are modelled after the project setup. This means the structural walls, floor slabs, roof surfaces and columns that outline the general form and load-bearing structure of the terminal building. These are the majority of the model geometry and the most influential in any subsequent deviation analysis.

Once the main structure has been completed, the openings and the facade elements are added, such as windows, doors, curtain wall systems, and glazed panels. Facade glazing is a major component of the building envelope and an important element class for the purpose of change detection for a terminal building of this scale and type.

The material properties are then assigned to each element of the model. In Revit, materials are tied to element categories, and when you export the model, these are written into the MTL material library file that comes with the OBJ mesh. The change detection framework then parses the material group names embedded in the MTL file reflecting Revit's internal element category naming to classify each region of the BIM point cloud according to architectural element type . This step is thus not only aesthetic, it is what makes possible the per-class deviation analysis that separates this study from simpler point cloud comparison approaches.

3.2.2 Development of 3D GIS Model

The as-built 3D model of the terminal building of Bhogapuram Airport was generated using Agisoft Metashape Professional, a photogrammetric processing software that generates high-quality 3D spatial data from overlapping imagery and point cloud data. The processing was made up of a sequential workflow, as shown in Figure 3.2 and described step by step below;

Import Image

The workflow starts with the loading of the captured data into Metashape. RGB images from the RFly drone camera were added to a new chunk using the Add Photos option in the Workflow menu. Then the LiDAR point cloud data was imported using Import Point Cloud option and both the data were processed together in the same project. All data were organised in a single chunk to preserve a consistent spatial reference during processing.

Image Registration

For the image alignment the Align Photos function from the Workflow menu was used. Metashape uses a scale-invariant feature matching algorithm to find common feature points among overlapping images, finds correspondences among image pairs, and estimates the camera pose (position and orientation) of each photograph in three-dimensional space (Agisoft LLC, 2023 and Chiabrando et al., 2020). The accuracy was set to High for this study in order to maximise the quality of the sparse point cloud and camera network. The alignment yields a sparse point cloud and a set of camera locations which are the geometric backbone of the reconstruction.

Checking and marking GCP

The model was georeferenced and systematic alignment errors were corrected by means of five ground control points. The GCPs are organised in the Reference panel in Metashape. Because the control points are manually identified and marked in several overlapping images using the marker placement tool, The actual coordinates of each GCP measured in the field and recorded in WGS84 were then entered in the Reference panel. The model was then updated by clicking Optimise Cameras in the Reference panel, which adjusts the camera network to minimise the reprojection error between the marked image positions and the real-world coordinates of the GCPs, once all five points had been marked and their coordinates assigned. This step is vital in making sure the reconstructed model is correctly anchored to real-world geographical coordinates.

Point cloud creation

Then, after alignment and georeferencing, the dense point cloud was created with the Build Point Cloud function in the Workflow menu. Metashape uses a multi-view stereo algorithm that looks at depth information from multiple overlapping image pairs to create a dense point cloud with a lot of geometric detail of the scene (Agisoft LLC, 2023). Quality was set to High, with Mild depth filtering to balance reconstruction detail and noise. The point cloud produced represents the surface geometry of the terminal building and the surrounding site at a level of detail consistent with the 0.05 m ground sampling distance of the aerial survey.

Deep filtering

When generating dense point clouds in Metashape, depth filtering is applied to manage how the software handles inconsistent depth estimates from different image pairs. The filtering process removes spurious and noisy points resulting from reflective surfaces, poorly textured regions or occlusion boundaries. An Aggressive filter was chosen for this study to remove obvious outliers while maintaining fine geometric detail on the building surface, a balance that is important to maintain accuracy in the subsequent deviation analysis.

Ground removal based on classification

At this stage, the dense point cloud also contains the ground surface, site infrastructure and other non-building features around the terminal building. The building geometry was isolated by using the Classify Point Cloud function under the Tools menu in Metashape to identify and remove ground points. It uses an algorithm that discriminates points belonging to the ground surface, based on local surface slope and elevation, from points belonging to above-ground structures. Then, the ground class was deselected, leaving only the building point cloud for the next step of mesh generation.

3D mesh model creation

Then the filtered point cloud was used to generate a three dimensional surface mesh using the Build Mesh function in the Workflow menu. The source data was set to Dense Cloud and the surface type was set to Arbitrary to allow for the complex non-terrain geometry of the terminal building. The face count was set to High to keep enough geometric detail. Metashape creates a continuous triangulated mesh surface from the point cloud. This provides a watertight representation of the building geometry.

Texture synthesis and hole filling

The mesh was textured using the Build Texture function on the Workflow menu. Metashape projects the original RGB images onto the surface of the mesh, assigning the colour values of the pixels from the drone photographs to the corresponding triangles of the mesh. The mapping mode was set to Generic and blending mode was set to Mosaic, to create a seamless and visually consistent texture over the entire surface of the building. Enable Hole Filling was also selected in the same Build Texture dialogue box. This interpolates colour and geometry across the missing areas to fill any remaining gaps or voids in the textured mesh, often caused by occluded surfaces, reflective glass facades, or areas of insufficient image overlap. This is particularly relevant for airport terminal buildings because of the large amount of glazed curtain wall and roof overhang surfaces that are likely to produce voids during photogrammetric reconstruction. Texture is not directly used for geometric deviation analysis, but provides a visually understandable as-built model. The hole-filled mesh ensures geometric completeness before export.

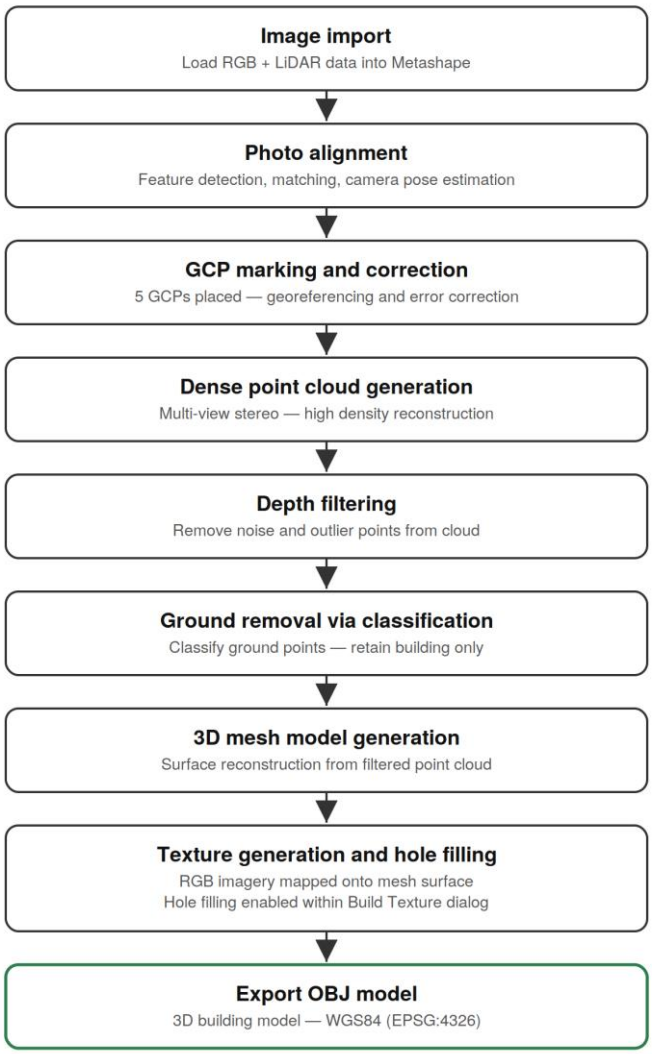


Figure 3.2: Workflow of 3D GIS model generation in Agisoft Metashape Professional.

3.2.3 Change Detection Processing Flow

65

The change detection framework developed in this study takes the BIM model and the 3D GIS model as input and processes the models through a sequential pipeline that results in a quantitative, element level comparison of design intent versus as-built reality. The pipeline, illustrated in figure 3.3, is composed of eleven distinct stages, from the data loading to the report generation. The phases are presented below with the mathematical formulation governing the crucial computational steps.

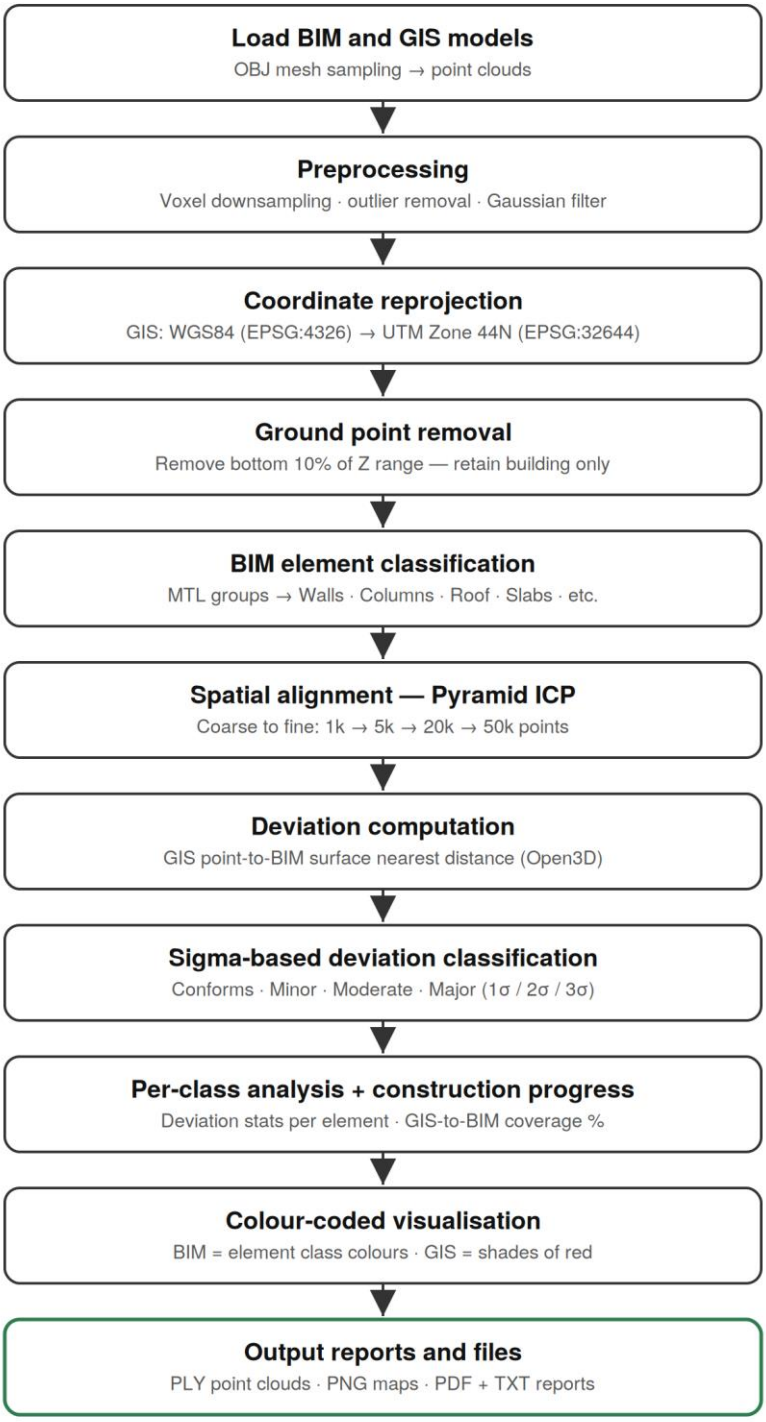


Figure 3.3: Processing pipeline of change detection in BIM–GIS.

67

Import BIM and GIS Models

The BIM and GIS datasets are both delivered as OBJ mesh files. We load each mesh in Open3D and sample the mesh by uniform surface sampling to get a point cloud. The number of sample points is set to be proportional to the number of vertices of the mesh, bounded by 500K points, to ensure that the resulting point cloud is geometrically representative of the original mesh surface and computationally affordable.

Pre-Processing

Each point cloud undergoes three sequential preprocessing steps.

Voxel downsampling divides the point cloud into a regular 3D grid of voxels with side length **v=0.05** m. All points within an occupied voxel are replaced by their centroid. This reduces point density while preserving spatial coverage.

4

Statistical outlier removal finds and removes noise points. We compute the mean distance of each point p to its k=20 nearest neighbours. Outliers are points whose mean neighbour distance is larger than the global mean by more than 3 standard deviations, and are removed:

Delete point p $if\ \bar{d}(p) > \mu d + 3 \cdot \sigma d$

Where, $\bar{d}(p)$ is the average distance from p to its k nearest neighbours, μd is the global mean of all such distances and σd is the corresponding standard deviation.

Gaussian spatial filtering smooths the residual scan noise by replacing a random 30% of points by the Gaussian-weighted average of their k=20 nearest neighbours. The weight given to each neighbour at distance d is:

$$w(d) = \exp(-d^2/2\sigma^2)$$

Where, σ = 0.075 m is the Gaussian kernel width (chosen to be 1.5× the voxel size). The filtered position of a point pi is a weighted average of its neighbours. $\hat{p}i = \Sigma\ wj \bullet pj\ \Sigma\ wj$ The overall cloud structure is maintained with localised noise removed by filtering only a portion of the points.

Coordinates re-projection

The GIS model is provided in WGS84 geographic coordinates (latitude φ, longitude λ, EPSG:4326). These have to be transformed into a metric Cartesian system before any spatial comparison can be made. The WGS84 coordinates are reprojected to UTM Zone 44N (EPSG: 32644) using the Transverse Mercator projection which is the appropriate projected coordinate reference system for the Bhogapuram site. The Easting (E) and Northing (N) coordinates are computed from the geodetic latitude and longitude using the standard UTM transformation:

$$E = k_0 \cdot N' \cdot [\, A + (1 - T + C) \cdot A^3/6 + \ldots \,] + 500{,}000$$
$$N = k_0 \cdot [\, M + N' \cdot \tan\varphi \cdot (\, A^2/2 + (5 - T + 9C + 4C^2) \cdot A^4/24 + \ldots \,) \,]$$

Where, $k_0 = 0.9996$ is the central scale factor (Pyproj Contributors, 2023), N' is the radius of curvature in the prime vertical, M is the meridional arc, $T = \tan^2\varphi$, $C = e'^2 \cdot \cos^2\varphi$, $A = \cos\varphi \cdot (\lambda - \lambda_0)$, and e' is the second eccentricity of the reference ellipsoid (WGS84: a = 6,378,137 m, f = 1/298.257). This conversion is done using the PyProj library when available, and falls back to a built-in implementation when PyProj is not installed.

Ground point deletion

The GIS point cloud at this stage is not only the terminal building but the ground surfaces, site infrastructure and surrounding terrain. A Z-axis threshold is used to remove the non-building points. Given the minimum elevation Zmin and maximum elevation Zmax of the entire cloud, a cutoff elevation Zcut is defined as:

$$\mathbf{Zcut = Zmin + a*(Zmax - Zmin)}$$

Where $\alpha = 0.10$, such as the bottom 10% of the vertical range is labelled as ground and removed. All points with z<=zcut are discarded. This simple but effective approach removes the majority of ground-level points while retaining the building structure above.

BIM element classification

The BIM point cloud is classified by architectural element type using the material group names embedded in the MTL file that accompanies the Revit OBJ export. Each material group name is parsed and matched to one of ten predefined element classes Wall, Roof, Column, Ceiling, Floor, Window, Door, Beam, Slab, and Misc through a keyword lookup table derived from Revit's internal category naming conventions.

Each vertex in the OBJ mesh is assigned the class of the material group active at the time the face referencing that vertex was defined. These per-vertex labels are then transferred to the sampled point cloud using a nearest-neighbour (NN) assignment. For each sampled point p in the BIM point cloud, its class label, c(p) is assigned as:

$$c(p) = c(\, \mathrm{argmin}_{v \in V} \| p - v \| \,)$$

Where, V is the set of OBJ mesh vertices and c(v) is the material class label of vertex v. The nearest neighbour query is implemented using a KD-tree for computational efficiency. Only element classes that have at least one associated point in the BIM cloud after sampling are designated as active classes; all others are excluded from reporting.

Spatial alignment; Pyramid ICP

The BIM model exists in local model coordinates and must be spatially registered to the GIS cloud before any deviation can be measured. This is achieved through a pyramid Iterative Closest Point (ICP) procedure operating at four successive levels of point density: 1,000 → 5,000 → 20,000 → 50,000 points (Besl & McKay, 1992). At each level, the algorithm iteratively minimizes the sum of squared distances between matched point pairs.

At each iteration, for a source cloud S and target cloud T, the optimal rotation matrix R and translation vector t are found by solving:

$$(R^*, t^*) = \mathrm{argmin}_{R,t} \Sigma_i \| R \cdot s_i + t - \hat{t}_i \|^2$$

Where, $s_i \in S$ and $\hat{t}_i \in T$ is the nearest point in T to the transformed s_i. The closed form solution is obtained by using the Singular Value Decomposition (SVD). For the centred matrices $S' = S - \mu S$ and $T' = T - \mu T$ the cross-covariance matrix $H = S'^T T'$ is decomposed as $H = U\Sigma V^T$ (Umeyama, 1991) yielding:

$$R = V^T U^T$$
$$t = \mu_T - R \cdot \mu_S$$

If $\det(R) < 0$, we negate the last column of V to get a proper rotation. In each iteration, the influence of outlier correspondences is suppressed by considering only the closest 80th percentile of matched pairs (in terms of distance). The algorithm terminates when the change in RMSE between successive iterations is below a convergence threshold τ, which is tightened from 10^{-3} at the coarsest level to 10^{-6} at the finest:

$$RMSE = \sqrt{((1/n) \cdot \Sigma_i \| R \cdot s_i + t - \hat{t}_i \|^2)} < \tau$$

The coarse-to-fine pyramid strategy eliminates a common failure mode of single-resolution ICP, which is to converge to local minima. This is done by establishing a globally consistent alignment at low point density, then refining it at higher density. The alignment quality is further evaluated using a pseudo-fitness metric, i.e. the percentage of source points within 5 times the final RMSE of the closest target point, giving a normalised [0,1] measure of the quality of the overlap.

Calculating deviation

The geometric deviation of each GIS point to the BIM reference surface is calculated as the Euclidean distance between the GIS point and the closest point in the BIM cloud after the alignment. Let q be a GIS point and B be the aligned BIM point cloud:

$$d(q) = \min_{b \in B} \| q - b \|_2$$

This operation is performed for each point in the aligned GIS cloud by the built-in open3d.compute_point_cloud_distance function. This function internally uses a k-d tree for an efficient nearest-neighbour lookup. The result is a deviation array d of length NGIS, where each element is the local deviation of the as-built surface from the BIM reference at that point (Open3D Development Team, 2023).

Sigma-based Classification of Deviations

Instead of a single, fixed tolerance threshold, deviations are categorised under a statistical sigma scheme. The mean μ and standard deviation σ of the deviation array d are first computed:

$$\mu = (1/N) \cdot \Sigma_i \, d_i$$
$$\sigma = \sqrt{((1/N) \cdot \Sigma_i \, (d_i - \mu)^2)}$$

A standardised Z-score is computed for each point:

$$z(d_i) = (d_i - \mu) / \sigma$$

Each GIS point is then assigned to one of four deviation classes based on the absolute value of its Z-score:

Conforms: $|z| \leq 1\sigma$ $(d_i \leq \mu + 1\sigma)$
Minor: $1\sigma < |z| \leq 2\sigma$ $(\mu+1\sigma < d_i \leq \mu+2\sigma)$
Moderate: $2\sigma < |z| \leq 3\sigma$ $(\mu+2\sigma < d_i \leq \mu+3\sigma)$
Major: $|z| > 3\sigma$ $(d_i > \mu+3\sigma)$

For a perfect Gaussian distribution 68.3% of the points would be in the Conforms band, 27.1% in Minor, 4.3% in Moderate and 0.3% in Major. Deviations from this expected distribution indicate the presence of systematic construction discrepancies, localised errors, or alignment residuals.

Per-class analysis and construction progress

Each GIS point is assigned to the BIM element class of the closest BIM neighbour, so that deviation statistics can be reported separately for each architectural element type. The class label for a GIS point q is:

$$c(q) = c(\operatorname{argmin}_{b \in B} \|q - b\|_2)$$

For each active element class k, the mean, median, standard deviation, maximum, and 95th percentile of the assigned deviation values are computed. These statistics allow class-specific conformance judgments to be made for example, distinguishing between well-constructed walls and significantly deviated roof surfaces.

The construction progress percentage P is computed as the fraction of BIM points that have a GIS scan point within a tolerance distance $\tau = 0.10$ m:

$$P = (|\{ b \in B : \min_{q \in Q} \|b - q\|_2 \leq \tau \}| / |B|) \times 100\%$$

Where, B is the set of BIM points and Q is the set of aligned GIS points. A BIM point is considered covered, i.e. physically constructed if at least one GIS scan point exists within τ metres of it. The resulting percentage provides a simple, interpretable estimate of overall construction completeness relative to the design model.

Colour-coded visualisation

The aligned BIM point cloud is rendered with distinct RGB colours per element class to visually distinguish architectural categories. The aligned GIS point cloud is rendered in a continuous red colour ramp, where the RGB value of each point is determined by its normalised deviation magnitude. The 99th percentile serves as a cap to normalise the deviation value d(q) to [0,1]:

$$\tilde{d}(q) = clip((d(q) - d_{min}) / (d_{99} - d_{min}), 0, 1)$$

The normalised value $\tilde{d}$ is then mapped to a red ramp: $\tilde{d} = 0 \rightarrow$ light pink (#FFD6D6), $\tilde{d} = 0.5 \rightarrow$ medium red (#FF4040), $\tilde{d} = 1 \rightarrow$ dark crimson (#7A0000 through a piecewise linear interpolation in RGB space. This gives an intuitive visual encoding, where the amount of red is directly proportional to the amount of deviation at each location.

CHAPTER 4
RESULTS AND DISCUSSION

This segment is again classified on the basis of the objectives, these sub-topics are;

4.1 3D GIS Model and BIM Model

This section presents the results obtained at each stage of the 3D GIS model generation workflow in Agisoft Metashape, followed by a description of the BIM model as prepared for the change detection analysis. The outputs from each processing step are discussed in relation to the screenshots captured during the workflow, as shown in **Figures 4.1** through **4.7**.

4.1.1 Image Import and Dataset Overview

The photogrammetric dataset was loaded into Agisoft Metashape as a single chunk containing a total of 5,079 drone images acquired over the Bhogapuram Airport terminal building site. The images were captured on 8 December 2025 using the RFly drone equipped with an RGB camera at 4032 × 3024 pixel resolution, flying at 50 metres above ground level. **Figure 4.1** shows the project workspace at the point of image loading, with a representative aerial photograph of the terminal building displayed in the main view. At this stage, the images appeared in the workspace as unaligned the camera positions had not yet been estimated but the dataset was confirmed complete before processing began.

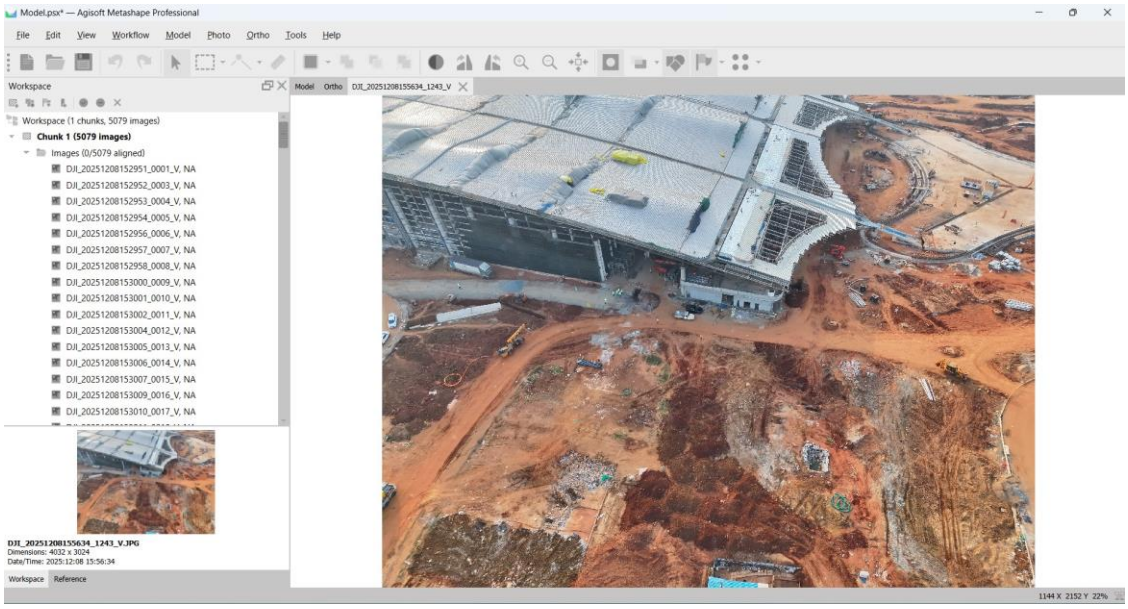


Figure 4.1: 5,079 images, 4032×3024 resolution and date 8 December 2025, unaligned at import stage.

4.1.2 Photo Alignment

Photo alignment was carried out using the Align Photos function with accuracy set to Highest. The advanced settings used a key point limit of 1,000 per megapixel and a tie point limit of 4,000, with generic preselection and reference preselection both enabled, and guided image matching activated to improve correspondence across low-texture areas. These settings, shown in **Figure 4.2**, were chosen to maximise the quality of the sparse point cloud and the robustness of the camera network particularly important given the large dataset size and the presence of uniform-texture surfaces such as the roof and cleared earth around the building.

The alignment completed successfully with all 5,079 images aligned a 100% success rate indicating good image overlap and consistent exposure conditions across the survey. This generated a sparse point cloud of 3,608,074 tie points covering the entire site extent as shown in **Figure 4.5**. This tie point density is consistent with what one expects from a Highest-accuracy alignment of a dataset of this size and provides a sound basis for dense reconstruction.

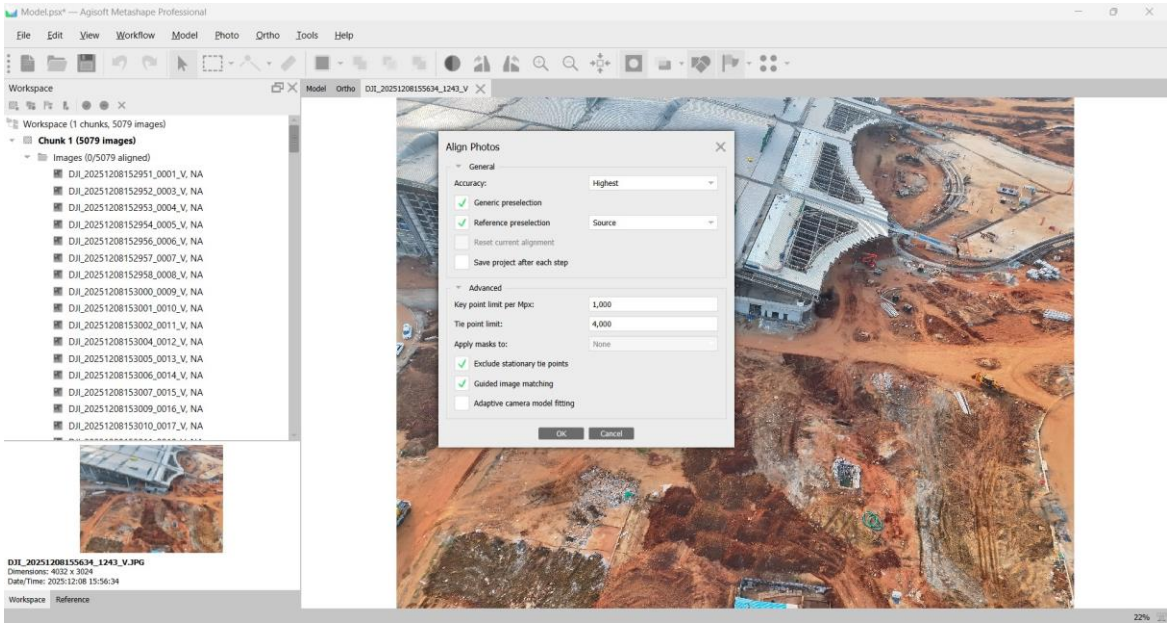
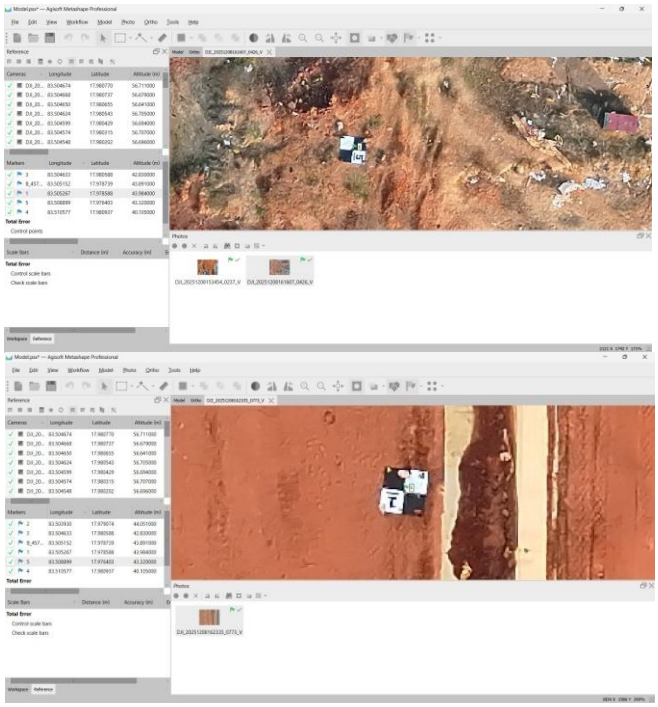


Figure 4.2: Align Photos settings: Highest accuracy, key point limit 1,000/Mpx, tie point 4,000, guided image matching on.

4.1.3 Geo-Referencing and GCP Marking

Five ground control points were located throughout the terminal building site prior to the drone flight and then marked in the Metashape Reference panel. **Table 4.1**: GCP coordinates The GCP coordinates are referenced in the WGS84 geographic coordinate system. **Figures 4.3 and 4.4** show the GCP marking interface. Markers were manually placed and pinned over a number of overlapping images. The markers were placed at different locations on the site with a longitudinal extent of around 83.504° to 83.511°E and latitudinal extent of 17.977° to 17.981°N, to have enough spatial coverage for georeferencing and to limit the reconstruction to the overall footprint of the terminal building.

The camera network was then optimised in the Reference panel to reduce the reprojection error between the marked image position and the GCP coordinates in the real world after marking the five GCPs on their respective sets of images. This step is the one that links the whole photogrammetric reconstruction to the real-world geographic space and it is what enables the final model to be used in a metric comparison with the BIM design model.



Figures 4.3 & 4.4: 5 GCPs + B_457, all exact coordinates pulled directly into **Table 4.1**.

Table 4.1: Coordinates of ground control points (WGS84).

GCP ID	Longitude (°E)	Latitude (°N)	Altitude (m)
1	83.505267	17.978588	43.984
2	83.503930	17.979074	44.051
3	83.504633	17.980588	42.830
4	83.510577	17.980937	40.105
5	83.508899	17.976403	43.320
B_457	83.505152	17.978739	43.891

4.1.4 Dense Point Cloud Production

A dense point cloud was generated from the complete dataset of 5,079 images with Ultra high quality depth maps with Aggressive filtering after alignment and GCP optimisation. The resulting point cloud shown in **Figure 4.6** contains 1,685,720,648 points that cover the complete airport site the terminal building, surrounding ground surfaces, access roads, and the active construction zones. The density of this cloud reflects the combination of high image overlap from the drone flight pattern and the Ultra high quality reconstruction setting, which processes depth information at full image resolution.

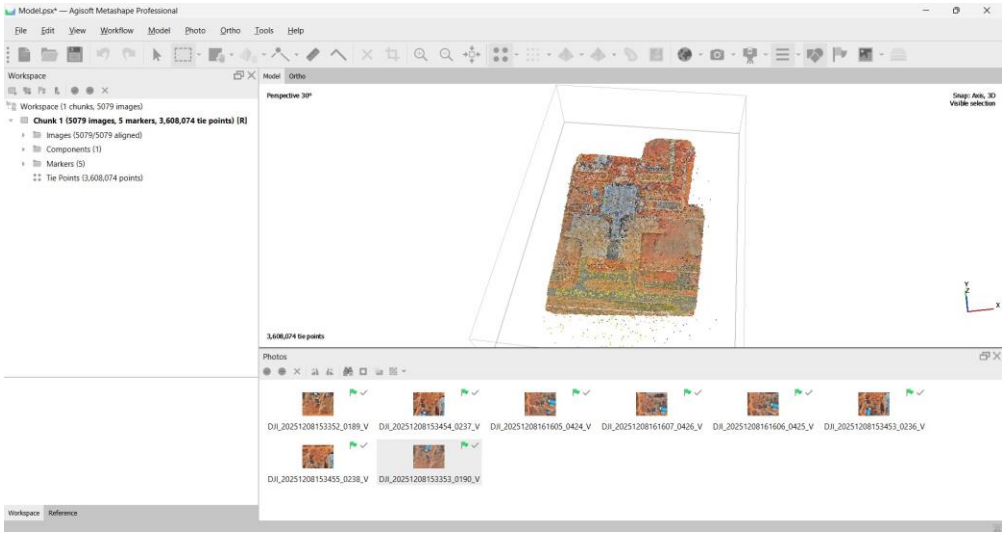


Figure 4.5: 5,079/5,079 aligned, 3,608,074 tie points.

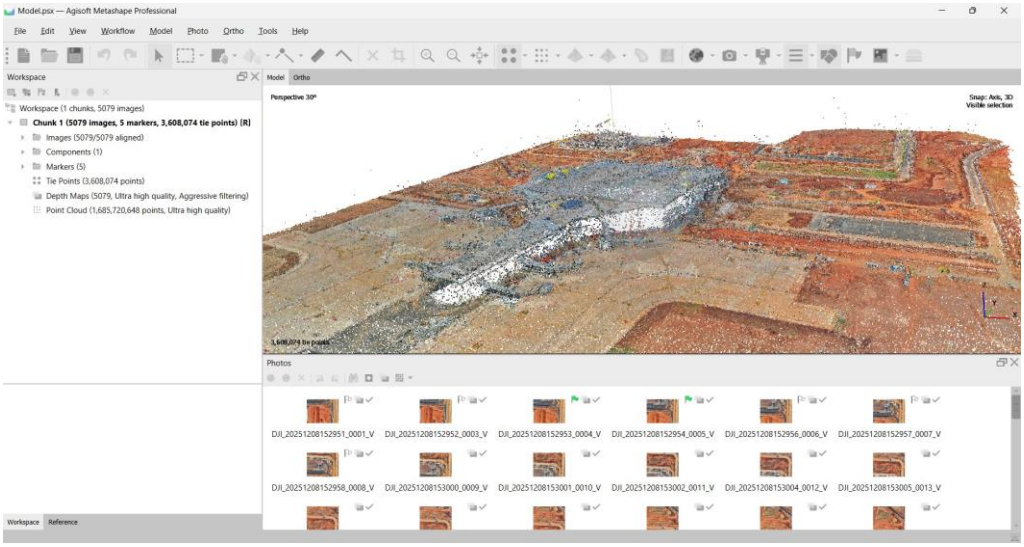


Figure 4.6: Dense point cloud: 1,685,720,648 points full site including ground and building.

With the full-site point cloud in place, ground classification was performed using the Classify Point Cloud function under the Tools menu in Metashape. This step separates ground-level points bare earth, site roads, construction debris, and other non-building surfaces from above-ground structural points belonging to the terminal building. Once classified, the ground class was deselected and the non-ground points were retained. This building-only point cloud, comprising 8,641,056 points, was then used to reconstruct the 3D mesh of the terminal structure. The classification and extraction step is important because including ground points in the mesh reconstruction would distort the building geometry and introduce significant errors in the subsequent BIM-to-GIS comparison.

4.1.5 Final 3D GIS Model; Building Mesh

The non-ground point cloud was used to reconstruct a three-dimensional surface mesh using the Build Mesh function, with source set to Dense Cloud, surface type Arbitrary, and face count set to High. **Figure 4.7** shows the final mesh of the terminal building, which contains 1,860,618 triangular faces and 929,420 vertices. The model captures well the form of the airport terminal - the large flat roof sections, the curved canopy overhangs, the central atrium and the finger pier extending from the main building body.

Openings or rough faces in the mesh represent areas of unfinished construction, especially on the building facades where structural elements were still under construction at the time of the December 2025 survey. This partial completion is precisely the condition that makes the change detection analysis meaningful a completed building

would tell you only what conforms or deviates; a partially built one also tells you what has not yet been constructed at all.

The mesh was exported in OBJ format with WGS84 geo-referencing (EPSG:4326) and forms the direct input to the Python-based change detection pipeline described in **Section 3.2.3**.

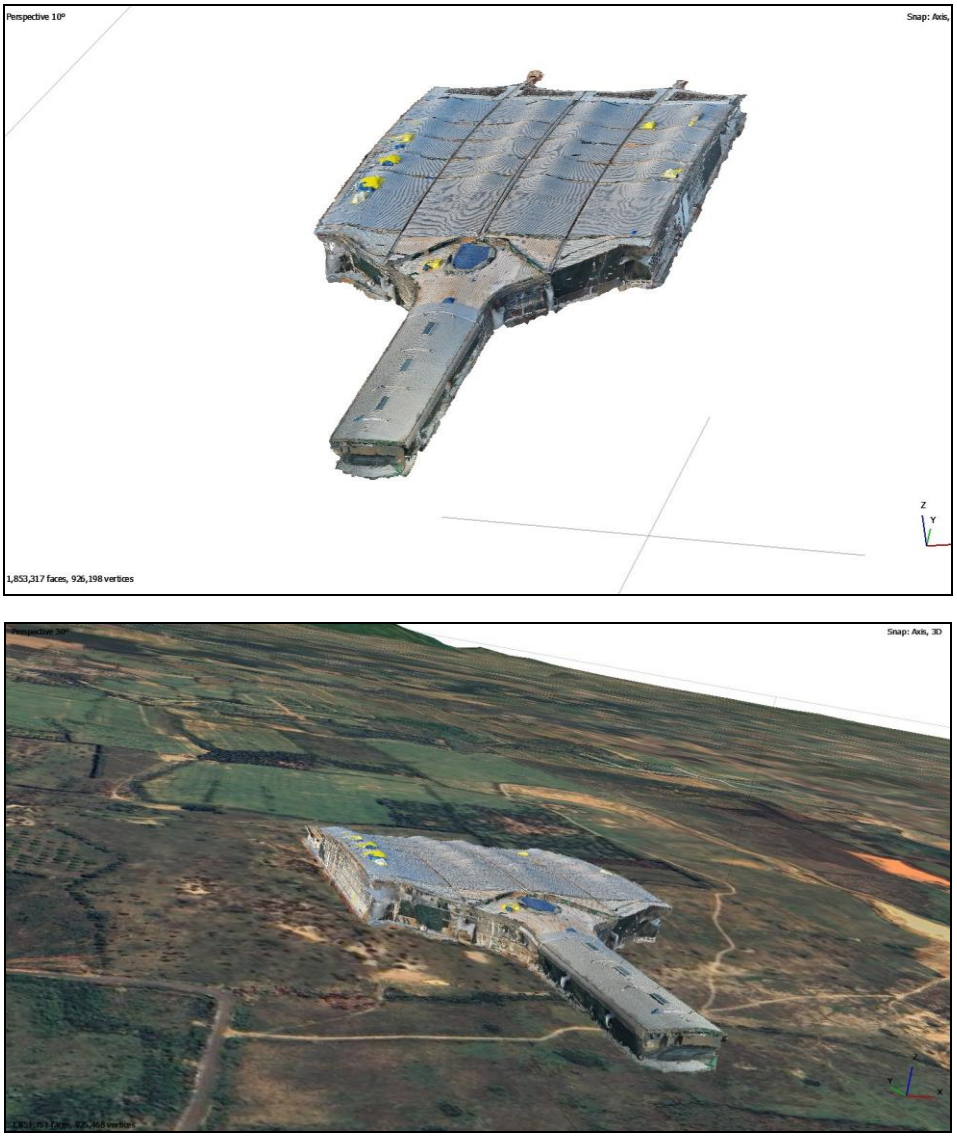


Figure 4.7: Final building mesh, 1,860,618 faces reconstructed from non-ground extracted point cloud with and without base(Google Satellites).

4.1.6 BIM Model: Autodesk Revit

The BIM reference model for the Bhogapuram Airport terminal building was prepared in Autodesk Revit 2026. The model was developed on the basis of the official airport master plan produced by RITES Limited (Airports Division), dated 03 February 2017, which defines the full spatial layout of the airport campus including the passenger terminal building, aircraft aprons, taxiways, and associated infrastructure. The master plan, shown in **Figure 4.8**, covers the Phase-I development area of 2004.52 acres at Vizianagaram district, Andhra Pradesh, and served as the primary design reference for the BIM model geometry.

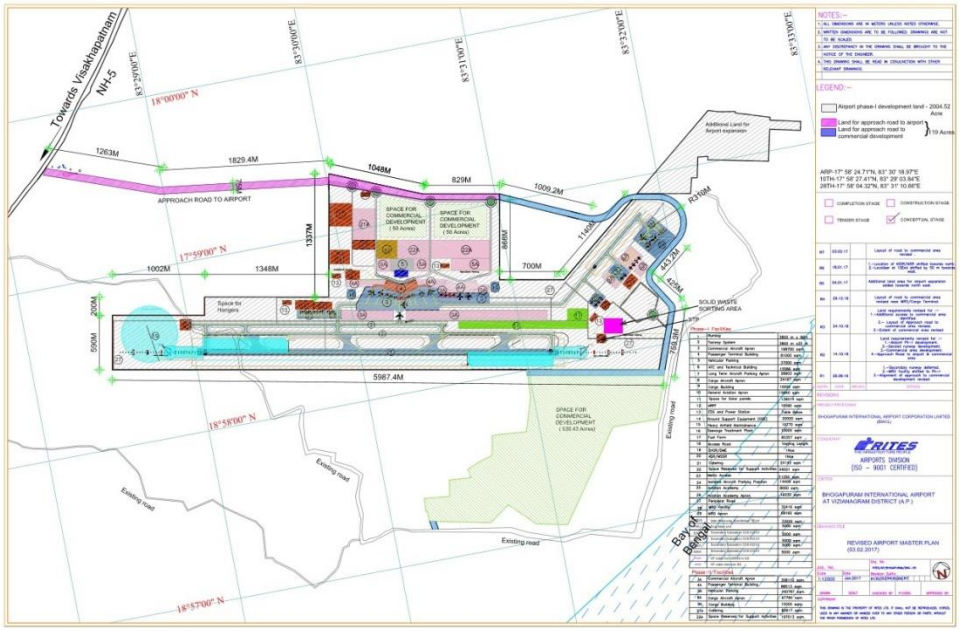


Figure 4.8: Revised Airport Master Plan, Bhogapuram International Airport, Vizianagaram District (RITES, 2017).

The BIM model focuses specifically on the passenger terminal building the structure that forms the subject of the change detection analysis in this study. The model was set up in Revit at a view scale of 1:100, with detail level set to Fine and architectural discipline, capturing the full structural form of the terminal at a level of resolution appropriate for geometric deviation analysis. **Figure 4.9** shows a 3D view of the terminal where its distinctive plan geometry is evident, with a wide main body with a protruding finger pier. The model structure is divided into five main categories of elements: Roof, Walls, Structural Framing (Beams), Ceiling, and Floor. Each category can be selected individually in Revit and has its own material assignment. Revit uses this to assign different visual colours per element type in the 3D view. The OBJ export keeps the categorical organization, which is the basis for element-level classification in the change detection analysis.

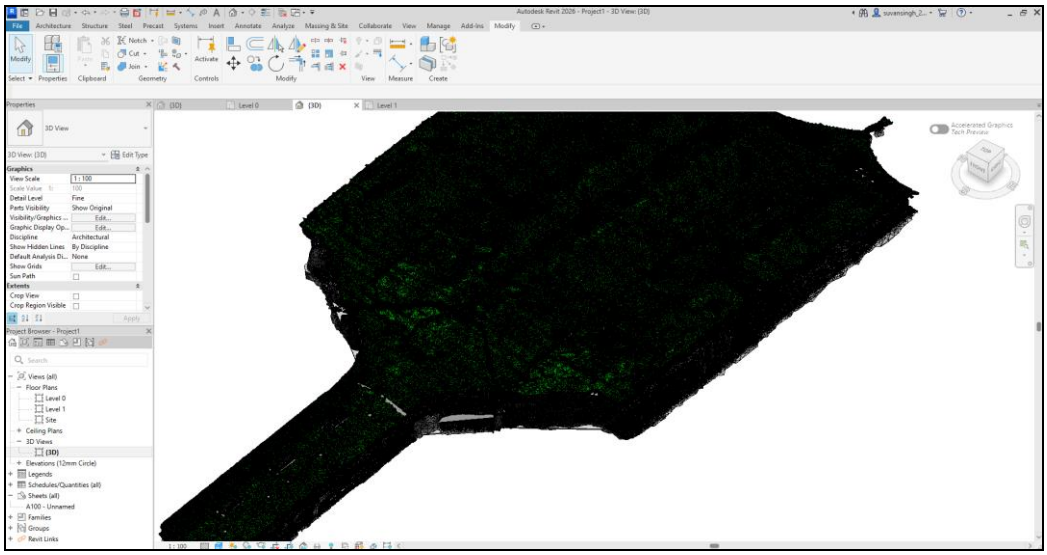


Figure 4.9: BIM model of the terminal building in Autodesk Revit 2026, 3D view 1:100, with the categories of the elements.

The model was exported from Revit as an OBJ file with the associated MTL material library. Each category of architectural element is written out as a named material group. The change detection framework parses these material group names (Roof, Walls, Structural Framing, Ceiling, Floor) to classify every point in the BIM point cloud to its element type, which enables the per-class deviation statistics reported in **Section 4.3**.

4.2 Point Cloud Statistics and Preprocessing

Once both datasets were loaded into the pipeline, the BIM model yielded 860,619 reference points after mesh sampling. The GIS model the photogrammetric reconstruction from the drone survey loaded with 698,968 points in total. Of these, 31,444 points were identified as ground level and deleted by the Z-axis cutoff filter, which deleted the lowest 10% of the vertical range below a cutoff elevation of −24.578 m. This resulted in 667,524 building points representing only the structural envelope of the terminal. The number of GIS points available for deviation analysis was 658,980 after spatial alignment and subsequent to post-alignment voxel downsampling at 0.05 m, which is the basis for all subsequent statistics.

The BIM model was scaled by a factor of 0.9652 m per native unit to convert from Revit's internal coordinate space to metric units. Gaussian spatial filtering was applied to both clouds with a kernel width of $\sigma = 0.075$ m, $k = 20$ neighbours, and a 70% random subset selection to suppress scan noise while preserving the overall point distribution.

The effect of Gaussian filtering on the point distribution is illustrated in **Figures 4.10 to 4.12**, which compare the pre-voxel cloud and the post-alignment cloud for the Z (Height), X (Easting), and Y (Northing) axes respectively. In all three axes, the left panel shows the raw pre-voxel clouds for BIM and GIS before any alignment each cloud is mean-centred so that spread rather than absolute coordinate value is compared. The BIM pre-voxel cloud has an original mean elevation of 17.8 m (local model space) and a standard deviation of 8.499 m, while the GIS pre-voxel cloud has a mean of −8.8 m (UTM height) and a standard deviation of 8.488 m almost identical spreads despite being in entirely different coordinate systems, reflecting the fact that both datasets represent the same building height range. The right panel shows the post-alignment distributions, where both clouds have been brought into the same metric space through control-point registration and ICP refinement. After alignment, the BIM cloud sits at a mean of −8.1 m with a standard deviation of 8.498 m, while the GIS cloud is at −8.4 m with a standard deviation of 8.108 m, a slight tightening in the GIS spread that reflects the Gaussian filter and voxel downsampling removing outlier points at the extremes of the height distribution. Similar convergence is visible in the X and Y panels, where the post-alignment BIM mean (765,430.7 m Easting) and GIS mean (765,429.0 m Easting) differ by less than 2 metres, consistent with the ICP RMSE of 0.53 m acting across a cloud with spatial extent of approximately 200 m.

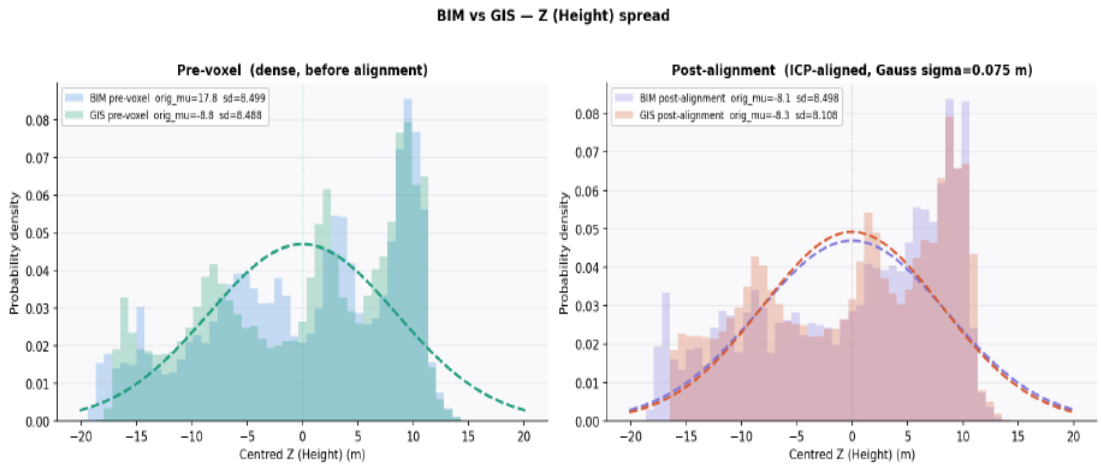


Figure 4.10: Point distribution comparison, Z (Height): pre-voxel (left) vs post-alignment Gaussian filtered (right).

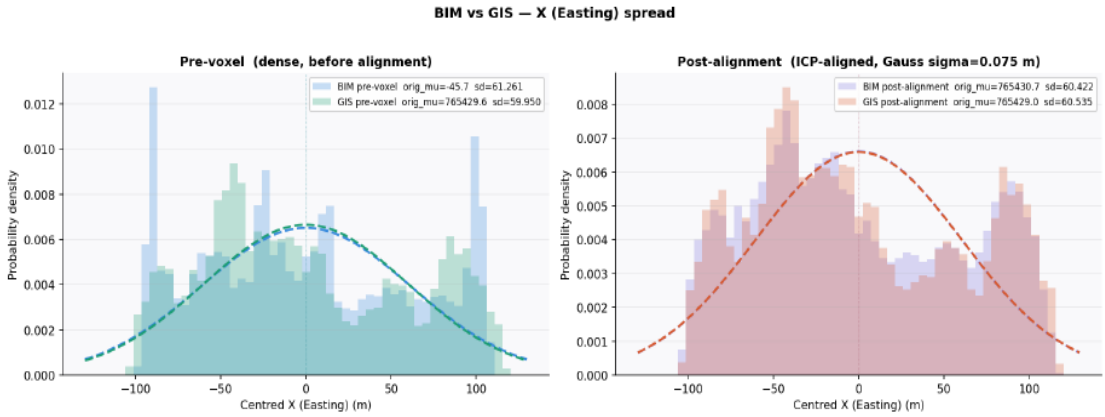


Figure 4.11: Point distribution comparison, X (Easting): pre-voxel (left) vs post-alignment Gaussian filtered (right),

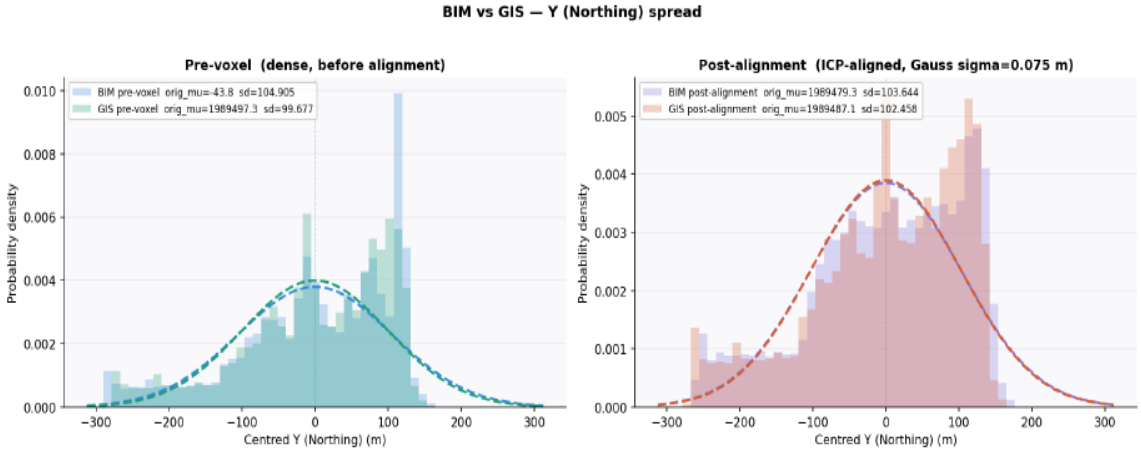


Figure 4.12: Point distribution comparison, Y (Northing): pre-voxel (left) vs post-alignment Gaussian filtered (right)

4.3 Spatial Alignment Results

Spatial alignment was performed using Mode 3, control-point georeferencing with Umeyama transformation followed by pyramid ICP refinement, operating in UTM Zone 44N (EPSG:32644). The alignment produced a pseudo-fitness score of 0.9906, which sits firmly in the Good band and indicates that well over 99% of the source points fell within five times the final RMSE of their nearest target point, a strong indicator of spatial overlap between the two datasets. The final ICP RMSE was 0.5289 m, rated as Moderate in the framework's quality banding.

The RMSE of 0.53 m is worth putting in context. It does not mean the alignment is poor; a fitness score of 0.99 contradicts that reading. Rather, it reflects the fact that

both datasets represent a partially constructed building, and there are inherent geometric differences between the BIM design surface and the as-built scan that no alignment procedure can eliminate. Part of what registers as RMSE is, in fact, the very deviation this study is trying to quantify. The four-view visualisation of the co-registered point clouds; Top, Bottom, Left, and Right views is shown in **Figures 4.13 to 4.16**, confirming that the BIM element classes and the GIS point cloud are spatially co-located across the full building footprint.

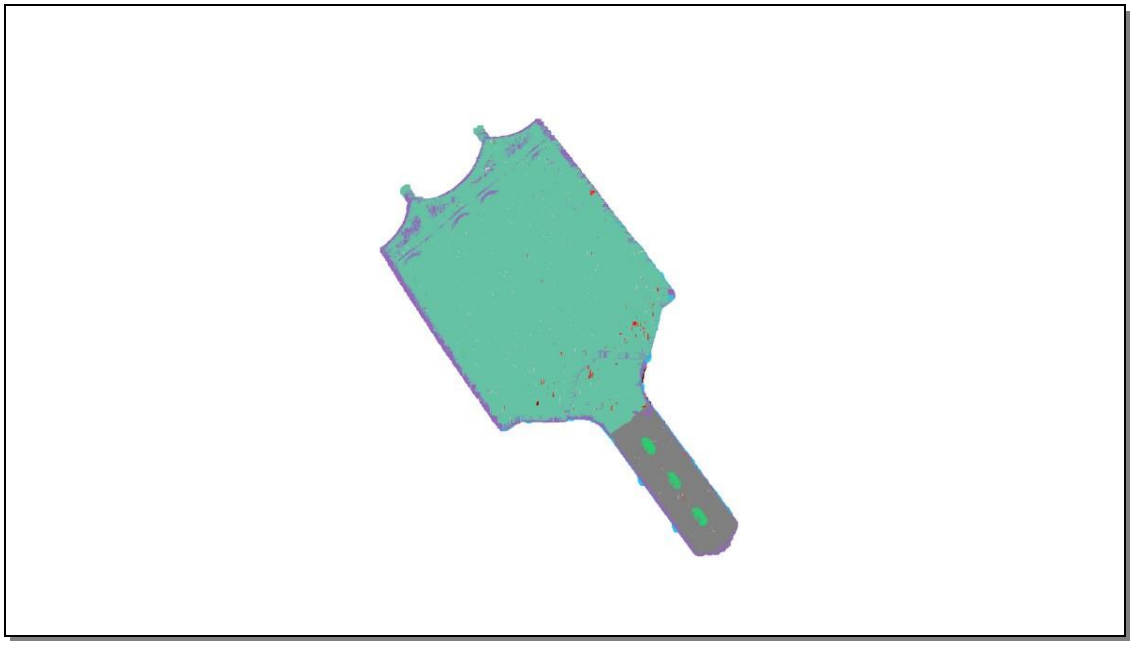


Figure 4.13: Top view: co-registered BIM element classes and GIS deviation point clouds.

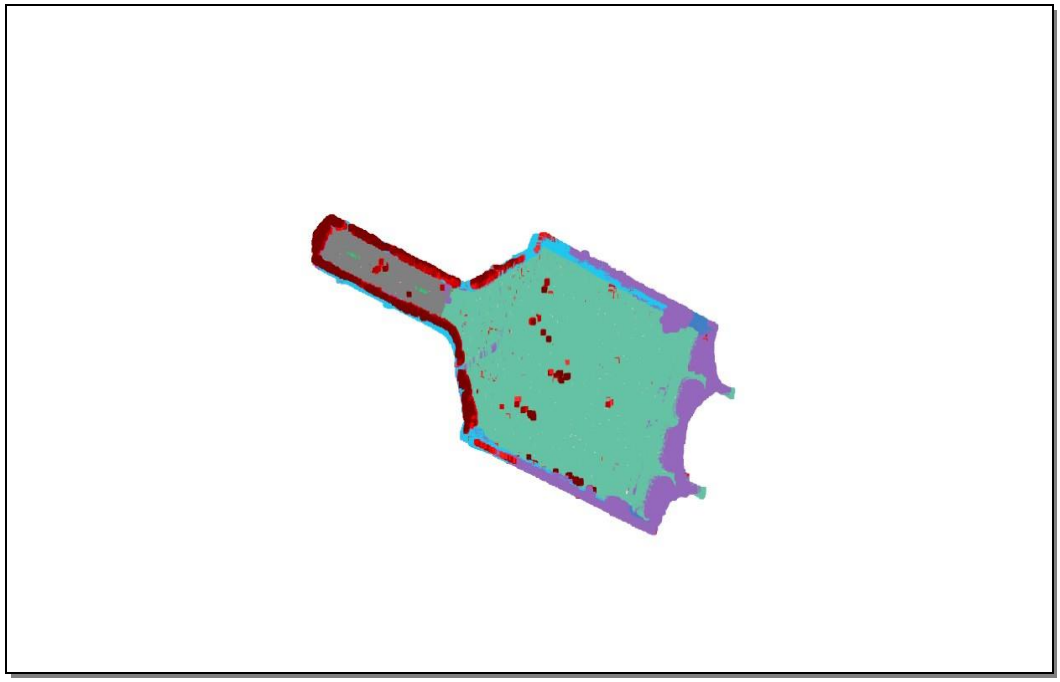


Figure 4.14: Bottom view: co-registered BIM element classes and GIS deviation point clouds.

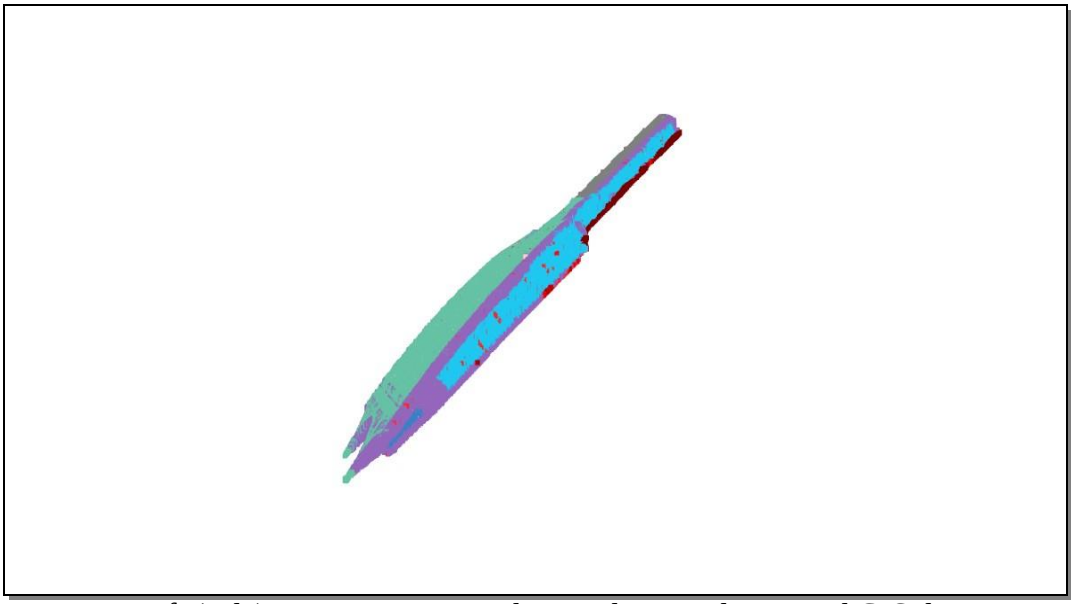


Figure 4.15: Left (side) view: co-registered BIM element classes and GIS deviation point clouds.

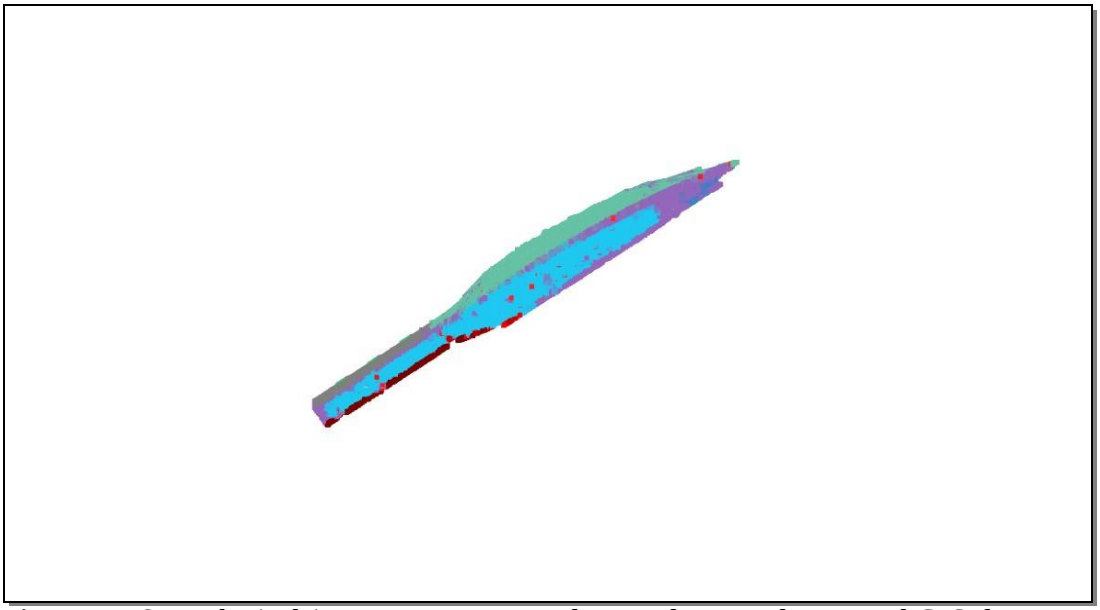


Figure 4.16: Right (side) view: co-registered BIM element classes and GIS deviation point clouds.

4.4 Deviation Analysis

4.4.1 Overall Deviation Statistics

The deviation of each GIS point from its nearest BIM surface was computed across all 658,980 analysed points. The mean deviation across the full dataset was 0.4226 m, with a median of 0.3820 m. The fact that the median sits slightly below the mean suggests a right-skewed distribution the bulk of points are tightly clustered at low deviations, with a smaller proportion of high-deviation outliers pulling the mean upward. This pattern is consistent with a structure where most of the building surface is reasonably well constructed but localised areas Edges, partially completed elements, exposed structural framing display larger discrepancies. The spread is reflected in the standard deviation of 0.3721 m. The deviation at the 95th percentile was 0.6554 m, which indicates that 95% of the scanned surface is within about 65 centimetres of the design model. The deviation at the 99th percentile was 2.036 m. The maximum recorded deviation of 8.77 m occurs at isolated locations and is most likely due to construction equipment, temporary structures or material stockpiles present in the scan but not represented in the BIM model.

4.4.2 Classification According to Sigma

The three band boundaries were identified as $1\sigma=0.7947$ m, $2\sigma=1.1667$ m, and $3\sigma=1.5388$ m using the sigma-based classification scheme with $\mu=0.4226$ m and $\sigma=0.3721$ m. The classification results are summarised in **Table 4.2** and illustrated in **Figure 4.17** (sigma pie chart) and **Figure 4.18** (deviation histogram).

Table 4.2: Sigma-based deviation classification results (μ = 0.4226 m, σ = 0.3721 m, n = 658,980).

Class	Z-score	Deviation boundary	Points	Area (m²)	%
Conforms	$\|z\| \leq 1.0\sigma$	≤ 0.7947 m	636,953	1,592.4	96.7%
Minor	$1.0\sigma – 2.0\sigma$	0.7947 – 1.1667 m	7,367	18.4	1.1%
Moderate	$2.0\sigma – 3.0\sigma$	1.1667 – 1.5388 m	3,964	9.9	0.6%
Major	$\|z\| > 3.0\sigma$	> 1.5388 m	10,696	26.7	1.6%
Total deviated	Minor + Moderate + Major	> 0.7947 m	22,027	55.1	3.3%

Area = point count × 0.05 m × 0.05 m (voxel size²)

The conformance rate of 96.7% is a remarkably high figure for a building still under construction. For comparison, a perfectly Gaussian deviation distribution would be expected to produce approximately 68% conformance at the 1σ boundary the fact that 96.7% of points fall within 1σ indicates the distribution is considerably more concentrated than a Gaussian model would predict, which is characteristic of a well-constructed structural shell where most surfaces are within the design geometry and deviations are localised rather than distributed uniformly.

The cumulative distribution curve, shown in **Figure 4.19**, rises steeply through the 0–0.8 m range before flattening near 97%, confirming that the overwhelming majority of the as-built surface lies within sub-metre deviation of the design. The long flat tail extending out to 8.77 m represents the small population of major deviation points discussed above.

4.4.3 Spatial Distribution of Deviations

The spatial hotspot map of mean deviation (**Figure 4.20**), plotted in UTM Zone 44N coordinates with X ranging from approximately 765,340 to 765,530 m Easting and Y from 1,989,230 to 1,989,650 m Northing, shows that the vast majority of the terminal building surface is rendered in light pink indicating low mean deviation generally under 1 m. Localised patches of deeper red, concentrated at the western edge near X ≈ 765,355, Y ≈ 765,545, and at a few interior locations, correspond to regions of higher mean deviation reaching 4–5 m. These hotspots are spatially consistent with the building's periphery and the finger pier junction areas where construction was at an earlier stage at the time of survey and where temporary formwork or exposed structural elements would create large geometric gaps relative to the finished BIM surface. The finger pier, which extends south from the main terminal body, exhibits moderate deviations along its length, probably because only the structural skeleton was present at the time of the December 2025 survey.

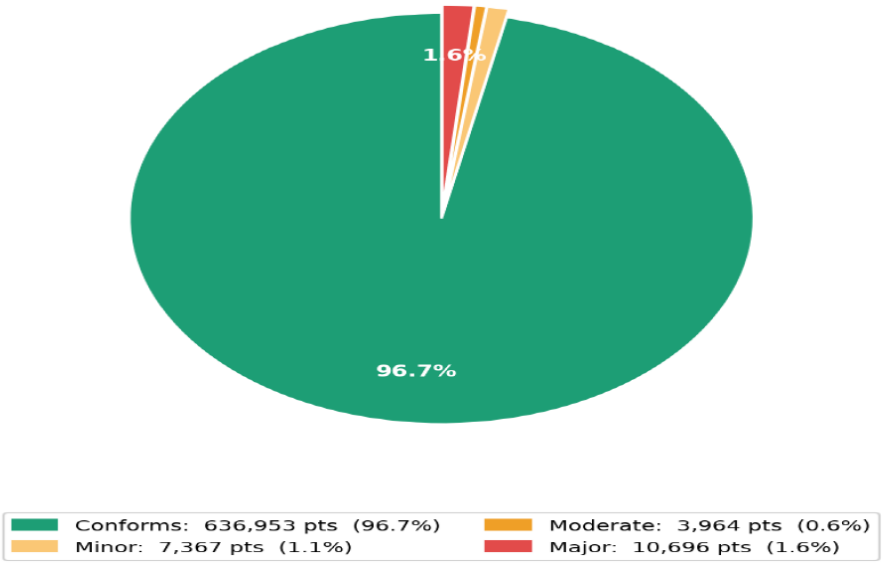


Figure 4.17: Classification of the sigma change pie chart (Conforms 96.7%, Minor 1.1%, Moderate 0.6%, Major 1.6%).

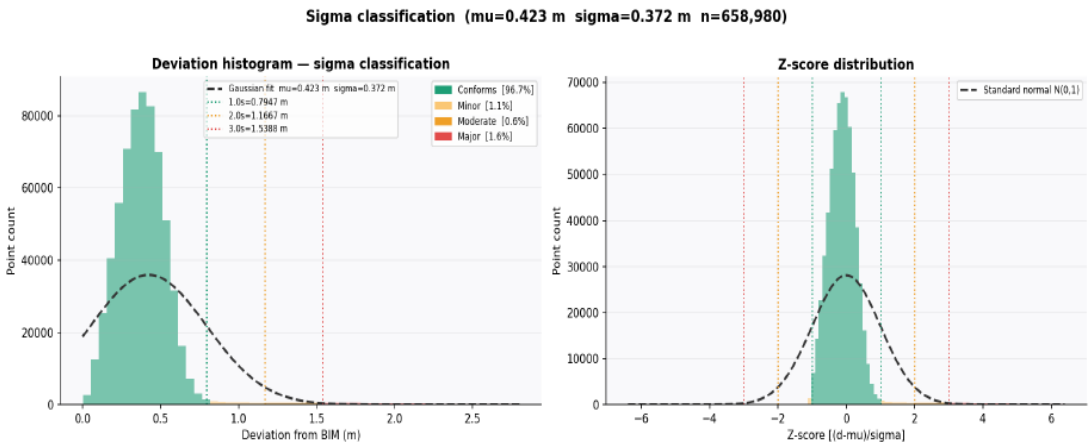


Figure 4.18: Histogram of deviations with sigma-band colour coding and Gaussian fit.

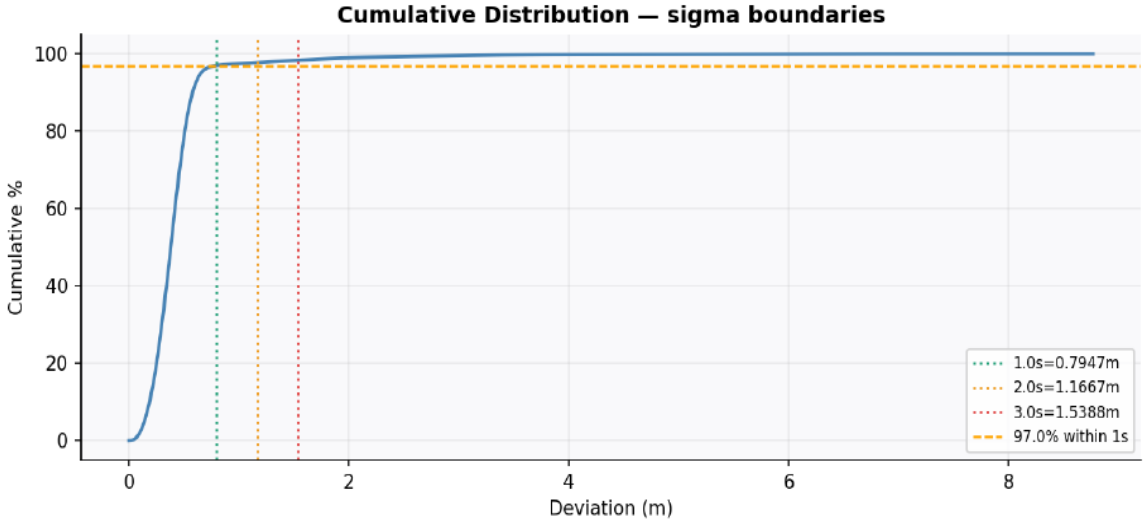


Figure 4.19: Cumulative distribution of deviations with 1σ, 2σ and 3σ limits.

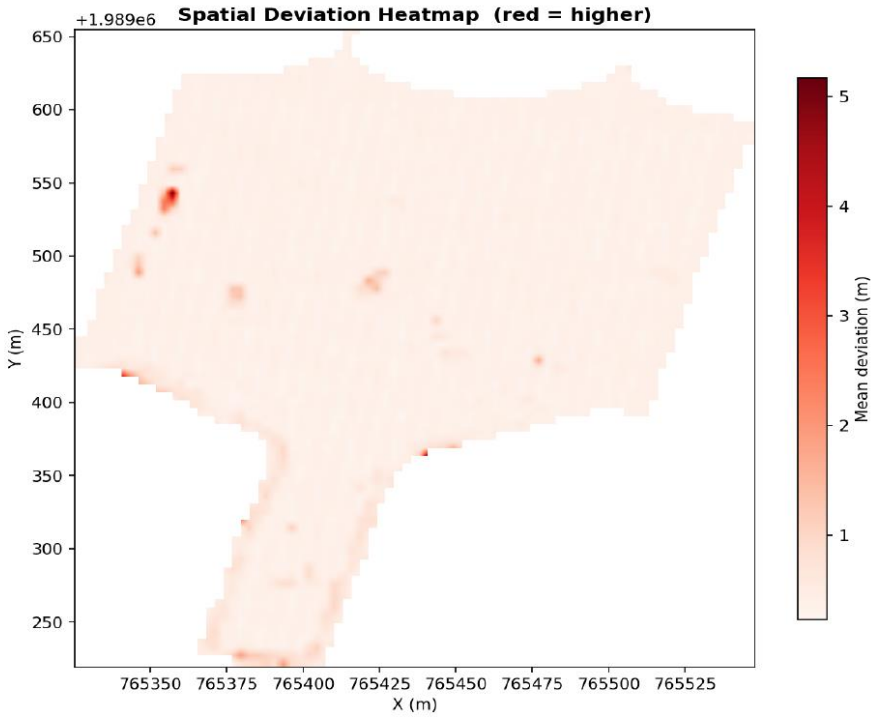


Figure 4.20: Hotspot map of spatial deviation (UTM Zone 44N; red = higher mean deviation).

4.5 Per-Element Class Deviation Analysis

One of the unique features of this framework is to report deviation statistics of each architectural element class separately that is identified in BIM model. The Revit MTL material groups identified six active classes of elements: Wall, Roof, Window, Beam, Slab, and Solar Panel. The complete statistics per class are given in Table 4.3. The bar chart of mean and max deviation per class is shown in **Figure 4.21**.

Table 4.3: Deviation statistics per BIM class.

Class	Count	%	Mean (m)	Max (m)	P95 (m)	Severity
Wall	14,726	2.2%	0.5826	6.9653	1.8926	Significant
Roof	355,059	53.9%	0.3778	3.8113	0.6045	Moderate
Window	112,933	17.1%	0.4617	8.1386	0.7380	Moderate
Beam	146,445	22.2%	0.4933	8.7692	1.1567	Moderate
Slab	28,688	4.4%	0.3818	4.1535	0.6178	Moderate
Solar Panel	951	0.1%	0.3728	0.6920	0.5953	Moderate

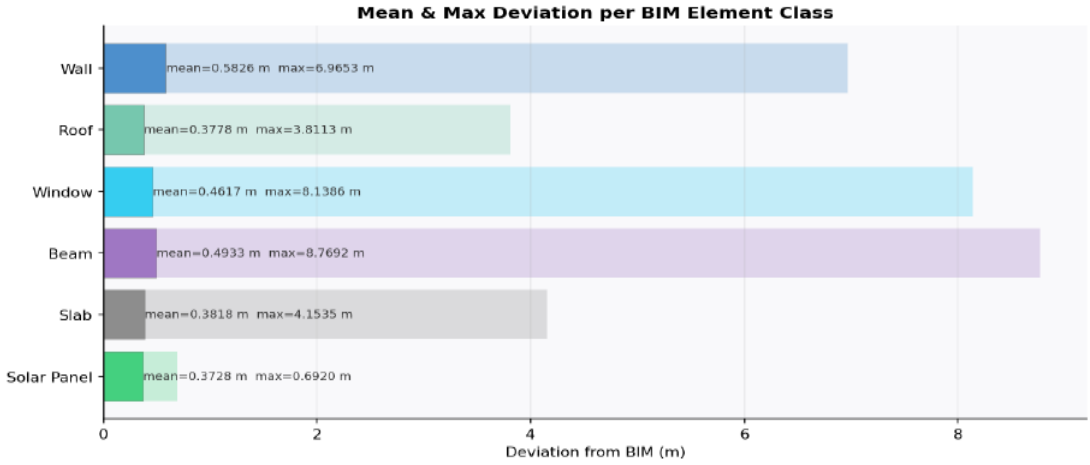


Figure 4.21: Mean and maximum deviation per BIM element class (bar graph).

The **Roof** is by far the most dominant element class, comprising 53.9% of all GIS points as the drone survey is capturing the building predominantly from above, which is understandable. Its mean deviation is 0.3778 m and P95 is 0.6045 m, again placing it firmly in the Moderate band. The relatively contained maximum of 3.81 m suggests that isolated roof surface patches deviate significantly, while the overall roof geometry is largely consistent with the design.

Beams are responsible for 22.2% of the points with an average deviation of 0.4933 m and max of 8.7692 m, the highest registered on all the element classes. Inherently, structural framing elements are difficult to match between BIM and as-built scan data as exposed beams under construction may be partially erected, temporarily braced, or obscured by formwork. A high maximum is consistent with locations where framing members in the scan do not have a completed equivalent in the BIM surface, rather than indicating a systematic construction error.

Windows represent 17.1% of points with a mean deviation of 0.4617 m and a maximum of 8.14 m. Glazed facade elements are notoriously difficult to reconstruct accurately from photogrammetry due to specular reflection and partial transparency, which can cause the photogrammetric surface to be reconstructed at the wrong depth or to contain holes (Xiao et al., 2023). The elevated maximum deviation for windows is therefore partly a measurement artifact of the survey method rather than a true construction error.

Wall is the only class rated as Significant, with a mean deviation of 0.5826 m and a P95 of 1.8926 m. Despite representing only 2.2% of total points, walls carry the highest mean deviation in the dataset. This is physically interpretable walls are vertical surfaces, and a nadir drone survey captures them obliquely or not at all. Any partially completed wall section will naturally generate large point-to-surface distances against the fully designed BIM wall geometry.

Slabs show the best overall performance of any major class, with a mean deviation of 0.3818 m, a P95 of 0.6178 m, and a maximum of 4.15 m. Horizontal floor slab surfaces, being well captured by the nadir-pointing drone camera and having a relatively flat design geometry, are the most accurately represented element type in the as-built scan relative to the BIM reference.

Solar Panels were detected as an active BIM class from the MTL groups an element type not initially anticipated in the element list representing just 0.1% of points (951 points). Their mean deviation of 0.3728 m and maximum of 0.6920 m suggest these small rooftop elements are well positioned relative to the design, with a tightly bounded deviation range consistent with precisely placed flat panel geometry.

4.6 Construction Progress Assessment

Construction progress was estimated by checking what proportion of BIM design points had a GIS scan point within a tolerance distance. Rather than applying an arbitrary fixed threshold, the tolerance was auto-scaled at runtime to the 1σ boundary of the actual deviation distribution (0.795 m) ensuring the progress metric is physically meaningful relative to the measured deviation characteristics of this specific dataset. Of the 103,928 BIM reference points, 100,686 were found to have at least one GIS point within 0.795 m, yielding a construction progress estimate of 96.88%.

A figure of 96.88% does not mean that 96.88% of the building has been physically completed to its final finished state. What it means, more precisely, is that 96.88% of the BIM design surface has a corresponding point in the GIS scan within the 1σ tolerance. Much of what this captures is the structural skeleton and roof of the terminal, which was substantially erected by December 2025. Facade cladding, interior finishes, glazing installation, and MEP systems none of which are captured by a photogrammetric exterior scan are not reflected in this figure at all.

The progress estimate is therefore best interpreted as a measure of structural shell completeness as visible from an aerial survey, rather than overall project completion. Within that interpretation, a figure approaching 97% is consistent with what the survey imagery shows a substantially erected main terminal structure with the roof in place across most of the footprint and the primary structural elements visible throughout the building.

29

4.7 Statistical Validation: Chi-Square Goodness-of-Fit Test

Table 4.4: Chi-square goodness-of-fit test results.

Metric	Value	Interpretation
Fitted distribution	Lognormal	Standard model for point cloud deviations
Chi-square statistic (χ^2)	33.5947	Goodness-of-fit vs lognormal
Degrees of freedom	16	17 bins − 2 fitted parameters
Critical value ($\alpha = 0.05$)	26.2962	—
p-value (χ^2)	0.0062	REJECT H_0 ($p < 0.05$)
Sample size (n)	5,000	Fixed subsample, seed = 42
Asymmetry check - BIM→GIS Vs GIS→BIM		
2-sample KS statistic	0.3472	REJECT H_0 - datasets are distinct
2-sample KS p-value	0.0000	Statistically significant difference
Cohen's d (effect size)	0.2998	Small effect (0.2 – 0.5)
Mean difference	116.4 mm	Practical asymmetry magnitude

64

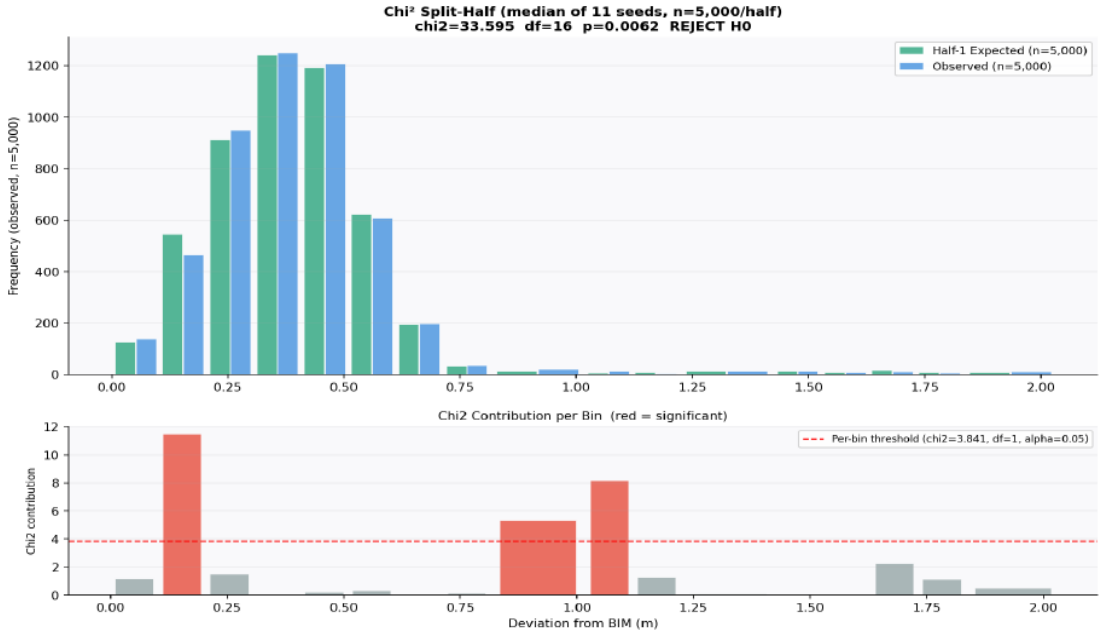


Figure 4.22: Chi-square goodness-of-fit: lognormal expected vs. observed, with per-bin contributions.

To assess the statistical character of the deviation distribution and the reliability of the BIM-to-GIS comparison, a chi-square goodness-of-fit test was applied to the full GIS-to-BIM deviation array (n = 658,980). A lognormal distribution was fitted to the data and used as the reference model, since point-cloud deviation arrays from photogrammetric surveys typically exhibit right-skewed, near-lognormal distributions (Qin et al., 2020 and Zhang et al., 2023). The test used a fixed subsample of n = 5,000 (seed = 42), with degrees of freedom adjusted to 16 to account for the two estimated distribution parameters.

The result was $\chi^2 = 33.5947$, df = 16, p = 0.0062 rejecting the null hypothesis that the observed deviation histogram follows a lognormal distribution at the 5% significance level. This finding does not invalidate the analysis but rather indicates that the distribution of deviations is more complex than a pure lognormal, as would be expected on a real construction site where different element types, different degrees of completeness and different scan quality over surfaces give rise to a mixture of distributions rather than a single clean parametric form.

The per bin chi-square contributions (Figure 4.22) indicate that a significant portion of the total chi-square statistic is concentrated in two bins, the 0.10-0.20 m range (contribution 11.47) and the 0.81-1.02 m range (contribution 5.33), and that the majority of the bins have negligible contributions less than the per bin threshold of 3.841. This local distribution implies that the distribution of deviations is lognormal-like over most of

its range, with deviations being inconsistent at specific magnitudes of deviation rather than broadly inconsistent.

In order to make sure that the BIM and GIS datasets are indeed different populations, a prerequisite for the change detection analysis to be meaningful, a two-sample Kolmogorov-Smirnov test was performed comparing BIM-to-GIS distances with GIS-to-BIM distances. The KS statistic of 0.3472 (p = 0.000) confirms the two distance distributions are statistically distinguishable so the comparison is not circular and there are real geometric differences between the two data sets. The practical effect size quantified by Cohen's d of 0.2998 is Small, with a mean difference of 116.4 mm between the two directional distance arrays. This small but statistically significant asymmetry is physically consistent with a partially constructed building where the BIM surface extends into regions not yet built the GIS cloud does not cover those areas, creating directional asymmetry in nearest-neighbour distances.

To check whether the BIM and GIS datasets are genuinely distinct populations a fundamental requirement for the change detection analysis to be meaningful a two-sample Kolmogorov-Smirnov test was applied comparing BIM-to-GIS distances against GIS-to-BIM distances. The KS statistic of 0.3472 (p = 0.000) confirms that the two distance distributions are statistically distinguishable, establishing that the comparison is not circular and that real geometric differences exist between the two datasets. The practical effect size is 0.2998 (Cohen, 1988) Cohen ' s d is Small and has a mean difference of 116.4 mm between the two directional distance arrays. This small but statistically significant asymmetry is physically consistent with a partially constructed building where the BIM surface extends into regions not yet built, the GIS cloud does not cover those areas, creating directional asymmetry in nearest neighbour distances.

39

CHAPTER 5
CONCLUSION

5.1 Conclusion

72

The objective of this study was to develop and demonstrate a systematic framework for integrating BIM and 3D GIS data to identify geometric changes in a building under construction by comparing what was designed and what was actually built. The Bhogapuram Airport terminal building served as the case study, and the results show that the approach is not only technically feasible but practically useful in a real, complex construction environment.

The framework brought together several components that individually exist in the literature but had not previously been combined in a single automated pipeline for this purpose. A drone-based photogrammetric survey of the terminal building was processed in Agisoft Metashape to produce a dense, georeferenced 3D mesh of the as-built structure. This was aligned with the Revit BIM model through a control-point georeferencing procedure followed by pyramid ICP refinement, achieving a pseudo-fitness score of 0.9906 confirming reliable spatial registration between the two datasets. Then, the distances of point-to-surface deviations were calculated for each of the analysed 658,980 GIS points, providing a comprehensive geometric comparison over the entire building footprint.

The sigma-based classification of these deviations showed that 96.7% of the as-built surface was within the Conforms band within 0.7947 m of design with only 3.3% of points classified as deviated in the Minor, Moderate or Major categories. This is a good result for a structure under construction, where geometric discrepancies from the final design model are introduced by scaffolding, partly completed elements and construction activity. The spatial hotspot map of deviations confirmed that the areas of highest deviation are concentrated at the building periphery and along the finger pier physically consistent with the least complete parts of the structure at the time of the December 2025 survey.

The elemental-level breakdown of deviations across Wall, Roof, Window, Beam, Slab, and Solar Panel classes provided a more nuanced picture than a single global statistic could provide. The Roof (53.9% of points) was the dominant feature for the dataset and exhibited moderate and well bounded deviations consistent with a substantially completed roof structure. The only class classified as Significant was the Walls with a mean deviation of 0.58 m. This is explained by the difficulty in capturing vertical surfaces from a nadir drone survey and the partially constructed state of the building facades. These element-level insights are just the sort of thing that a site engineer or project manager would need to prioritise corrective action and direct inspection resources efficiently.

The metric of construction progress automatically scaled to the boundary of the 1σ deviation estimated 96.88% of the BIM design surface as covered by the as-built scan, indicating the significant structural completion of the terminal shell at the time of survey. Statistical validation through chi-square goodness-of-fit test and two-sample Kolmogorov-Smirnov test confirmed the internal consistency of the deviation measurements and authenticity of distinctness between the BIM and GIS datasets establishing that the comparison is methodologically sound and not an artefact of the alignment process .

Overall, the results shows that the integration of BIM-GIS for change detection is possible, automated and informative at the scale of a real airport terminal building. The framework produces outputs colour-coded point cloud visualisations, spatial hotspot maps, sigma classification tables and per-element deviation charts that are directly interpretable by construction professionals without requiring specialised geospatial expertise. That accessibility is arguably as important as the technical accuracy; because a method that produces correct results but is too complex to act on has limited practical value.

5.2 Limitations of the Study

The framework yielded meaningful and interpretable results; however, several limitations were identified during the study that affects the scope of the findings.

Exterior only – Drone photogrammetry can only generate the exterior surface of the building. The drone is completely blind to interior spaces, internal walls, ceiling systems, floor slabs and MEP elements and these are outside the scope of the deviation analysis. Interior conditions would require handheld or backpack-mounted LiDAR scanners, which were out of scope of this study.

Single time point – The GIS dataset represents the site at a single point in time December 2025. The study thus conducts a design-to-reality comparison as opposed to a true temporal change detection. Repeated surveys at regular intervals would be needed to monitor the development of deviations over the construction programme.

Construction site clutter – Cranes, scaffolding, stockpiles of materials and temporary structures present on site at the time of survey are captured in the point cloud. These are not part of the building and cannot be always automatically separated from genuine structural elements. This is part of the Major deviation category.

No embedded georeferencing in BIM – The BIM model does not have any real-world coordinates embedded, so the alignment is completely dependent on the control-point ICP process. While this did yield a fitness score of 0.99, embedding a georeferenced project base point directly in Revit would allow for more reliable and deterministic future alignments.

These limitations do not invalidate the results, but define the boundaries within which they should be interpreted. The biggest improvements for future applications of this framework would be to handle interior capture with handheld LiDAR and to use a multi-temporal survey approach.

5.3 Recommendations for Future Work

The study naturally led to several directions for extending and improving the work. Interior capture with handheld LiDAR The main limitation of the current framework is that it is limited to exterior surfaces.

The use of **handheld or backpack mounted LiDAR scanners for interior capture** enables the inclusion of internal walls, floor slabs, ceiling surfaces and MEP spaces into the deviation analysis. The same processing pipeline would be directly applicable to interior point clouds and the extension would be technically straightforward once the data acquisition challenge is solved.

Multi-temporal monitoring – Repeating the drone survey regularly, at monthly intervals or at key construction milestones, would transform the framework from a one-off quality check, to a true construction monitoring tool. 4D BIM schedule could be checked for construction progress. Post-completion settlement or structural movement could be monitored throughout the operational life of the building.

Direct BIM georeferencing - The residual alignment uncertainty noted in the study would be removed and the registration made deterministic by embedding real world survey coordinates directly into the Revit project base point instead of using iterative ICP alignment. It's a relatively small change to the BIM authoring workflow but would make the deviation measurements much more reliable.

Automated removal of site clutter – By classifying permanent structural elements from temporary construction objects using machine learning or height-based segmentation, the deviation analysis contamination from cranes, scaffolding and stockpiles of materials will be reduced. Increasing the reliability of the Major deviation category as an indicator of real construction error.

Application to other building types - The framework was demonstrated on an airport terminal, but it is not site-specific by nature. Testing and demonstrating its generalisability on railway stations, hospital complexes, industrial facilities or multi-storey commercial buildings will help to identify any workflow adjustments required for different construction typologies.

The construction industry is moving, at varying speeds, to greater use of digital data in site management. Drone surveys are now routine, adoption of BIM is accelerating and the computational tools to bridge the two are becoming increasingly accessible. One working approach to that connection is contributed by this study: a pipeline that turns two standard digital outputs of a modern construction project into an automated, quantitative

assessment of how closely the building being built matches the building that was designed. There is still a long way to go before such analysis is part of everyday construction practice but the direction is clear and the results presented here indicate that the technical basis is sound.